*Clays and Clay Minerals*, Vol. 63, No. 3, 163–184, 2015.

# COMPOSITION AND GENESIS OF THE NICKEL-CHROME-BEARING NONTRONITE AND MONTMORILLONITE IN LATERITIZED ULTRAMAFIC ROCKS IN THE MURATDAĞI REGION (UŞAK, WESTERN ANATOLIA), TURKEY

Selahattin Kadir[1,*], M. Selman Aydoğan[2], Ömer Elitok[3], and Cahit Helvacı[4]

[1] Eskişehir Osmangazi University, Department of Geological Engineering, TR−26480 Eskişehir, Turkey
[2] Balıkesir University, Department of Geological Engineering, TR−10145 Balıkesir, Turkey
[3] Süleyman Demirel University, Department of Geological Engineering, TR−32260 Isparta, Turkey
[4] Dokuz Eylül University, Department of Geological Engineering, TR−35160 İzmir, Turkey

**Abstract**—Widespread lateritized ultramafic rocks in the southern part of the Muratdağı region of Turkey constitute a significant source of Ni-Cr-bearing ore with economic potential. However, no mineralogical or geochemical characterizations of these important materials have been performed previously. The aim of the present study was to describe the mineralogy, geochemistry, and genesis of Ni-Cr-bearing smectite in garnierite and ferruginous saprolite associated with the lateritized ophiolite-related ultramafic rocks. The lateritic zones are well developed over serpentinized harzburgitic mantle peridotites. The lateritized units and related bedrocks were examined using polarized-light microscopy, X-ray diffraction, scanning and transmission electron microscopies, and chemical and isotopic methods. The garnierite-containing saprolites are enriched in smectite, Fe-(oxyhydr)oxide phases, and opal-CT. Micromorphological images revealed that flaky smectite and, locally, Fe-rich particles, alunite, gypsum, gibbsite, and sulfur crystals developed along the fractures and dissolution voids. The development of saprolite demonstrates chemical weathering. The presence of silicified and Fe-(oxyhydr)oxide phases associated with gypsum, alunite, and local native sulfur in vertical and/or subvertical fractures and fault infillings are indicative of hydrothermal processes along the extensional, tectonically related fault systems. Chemical weathering and hydrothermal processes, which probably started during the Oligocene and Miocene, led to the formation of nontronite, Fe-bearing montmorillonite, and local Fe-rich kaolinite. Nickel and Cr are concentrated significantly in the saprolite zone and are positively correlated with $Fe_2O_3$ content, which is controlled by the formation of nontronite, montmorillonite, and Fe-(oxyhydr)oxide phases. Nickel-Cr-bearing nontronite and montmorillonite precipitated from alkaline water as a result of the increasing $(Fe_2O_3+Al_2O_3+Cr_2O_5+Ni+Co)/(MgO+SiO_2)$ ratio under the control of both chemical weathering and hydrothermal processes. The Fe and Mg (associated with Ni and Cr) required for the formation of smectite were supplied by solutions from both chemical weathering and hydrothermal alteration of Ni-Cr-bearing olivine and pyroxene in the harzburgitic bedrock; the Al was supplied by schists, granite, and volcanic units.

**Key Words**—Fe-(oxyhydr)oxide, Garnierite, Laterite, Montmorillonite, Muratdağı, Nontronite, Saprolite, Turkey, Ultramafics.

## INTRODUCTION

Supergene lateritic nickel deposits that formed in tropical humid climates from ultramafic rocks by chemical weathering processes often contain economically exploitable reserves of nickel and cobalt (Cornwall, 1966; Zeissink, 1969; Elias *et al*., 1981; Nahon and Colin, 1982; Freyssinet *et al.*, 2005). Based on their mineralogical compositions, Ni laterites are fundamentally classified as 'Type A' (talc, chlorite, sepiolite, serpentine), 'Type B' (nontronite and saponite), and 'Type C' (Fe-(oxyhydr)oxide phases, such as goethite and lepidocrocite) (Alcock, 1988; Brand *et al.*, 1998; Gleeson *et al*., 2003; Wells *et al.*, 2009). Among these, 'Type A' Ni deposits are common products of the chemical weathering of ultramafic units in southern Asia and the western United States, 'Type B' deposits are common in western Australia and the Ural Mountains, and 'Type C' deposits are found in western Australia, New Caledonia, Çaldağ (Manisa, western Turkey; Helvacı *et al*., 2007, 2008, 2013; and references therein), and Sarıçimen (Van, eastern Turkey; Çolakoğlu, 2009). Lateritized ophiolite-related ultramafic rocks are distinguished by their geological and lithological features, mineralogical assemblages, and chemical compositions along with the occurrence of Fe-(oxyhydr)oxide- and S-bearing sulfate ore phases, the micromorphologies of the clay and coexisting non-clay minerals, and their stable-isotope compositions (Çağatay *et al.*, 1981; Sheppard and Gilg, 1996; Brand *et al.*, 1998; Helvacı *et al*., 2007, 2008, 2013; Thorne *et al*., 2009). In addition, garnierite and lateritic zones have been studied with respect to their genesis and occurrences along with their chemical, mineralogical, and structural characteristics (Brindley and Maksimovic, 1974; Brindley *et al*., 1979; Decarreau *et al*., 1987; Elias, 2001a, 2001b; Gleeson *et al*., 2003,

* E-mail address of corresponding author:
skadir_esogu@yahoo.com
DOI: 10.1346/CCMN.2015.0630302

2004; Freyssinet *et al.*, 2005; Christidis and Mitsis, 2006; Wells *et al.*, 2009; Tauler *et al.*, 2009; Butt and Cluzel, 2013).

The Muratdağı region has been examined from different geological perspectives (Bingöl, 1977; Yıldız and Bailey, 1978; Gökçe and Spiro, 1994; Başarı, 1982; Aydoğan, 2006; Aydoğan *et al.*, 2008; Erkoyun and Kadir, 2011; Kadir and Erkoyun, 2013; Yüksel, 2013). Nickel-Cr-bearing smectite in laterites occurs abundantly in the reddish, yellowish, and green-colored saprolite zone over the serpentinized mantle peridotites in the southern part of the Muratdağı region in western Anatolia, Turkey. The genesis of Ni-laterites has been the subject of numerous previous studies (Nahon and Colin, 1982; Gleeson *et al*., 2003; Freyssinet *et al.*, 2005; Wells *et al.*, 2009; Helvacı *et al*., 2007, 2008, 2013; Butt and Cluzel, 2013). No information is available, however, about the clay mineralogy, or geochemistry, or about the genesis of the complex and heterogenic lateritic Ni deposits formed by the continuous weathering and hydrothermal processes of ultramafic rocks in this area, which probably started during the Oligocene and Miocene, respectively. The aim of the present study was to investigate the mineralogy, geochemistry, and genesis of Ni-Cr-bearing clay minerals within the saprolite zone containing garnierite. The study also provides new data and interpretations to guide future exploration of the chemical weathering and hydrothermal processes of ultramafic rocks and related lateritic ore deposits in similar geological areas.

## GEOLOGY OF THE MURATDAĞI AREA

The ophiolitic units of the Muratdağı region (Mt. Murat) occur within the central part of the İzmir-Ankara-Erzincan suture zone (Figure 1). The basement rock units of the Muratdağı region beneath the cover-rock series of the Menderes Massif consist of low-grade Paleozoic metamorphic rocks of the Baybuyan Formation, the Arıkaya Formation, the Upper Triassic Kırkbudak Formation, and the Jurassic Çiçeklikaya Formation. These rocks are intruded by the Miocene Baklan Granite (Aydoğan *et al.*, 2008; Figure 1). The Baybuyan Formation consists of marble, quartzite, amphibole schist, phyllite, garnet schist, biotite schist, muscovite-chlorite schist, quartz-muscovite schist, and chlorite-sericite schist and passes upward through the marbles of the Arıkaya Formation (Günay *et al*., 1986). The Kırkbudak Formation consists of metaconglomerate and metasandstone and is overlain unconformably by dolomitic limestones, and locally by jasperitic limestones of the Jurassic Çiçeklikaya Formation. These units are overlain tectonically by the Muratdağı ophiolite consisting of ophiolitic mélange and massive harzburgitic mantle peridotites. Nickel-rich laterite is well developed over the serpentinized peridotites of the Muratdağı ophiolite. The basement units and the Muratdağı ophiolite are overlain unconformably by Neogene deposits (Gökçe, 1987; Aydoğan, 2006; Karaoğlu and Helvacı, 2012). The absence of Eocene–Oligocene sedimentary deposits in the Muradağı region suggests that the region was subjected to uplift, fluctuation of the semi-arid climatic conditions, and chemical weathering (Şengör and Yılmaz, 1981; Yılmaz *et al*., 2000; Ersoy *et al*., 2014; Külah *et al*., 2014).

Regionally, the Muratdağı region is bounded by the Gediz-Alaşehir and Denizli grabens in the south and the Simav graben in the north, with northwest–southeast-striking normal fault systems (Figure 1). The pronounced normal fault systems are represented by a horst-graben system in which the grabens are filled by Neogene basin deposits (from west to east: Gördes, Demirci, Selendi, and Uşak-Güre basins) (Öner and Dilek, 1999; Seyitoğlu *et al*., 2000; Ersoy and Helvacı, 2007; Ersoy *et al*., 2011; Karaoğlu *et al*., 2010; Karaoğlu and Helvacı, 2012). Northwest–southeast, east–west, and northeast–southwest striking normal faults with strike slip components are observed in the Muratdağı region (Günay *et al*., 1986), which, along with its surrounding environment, make up a geothermal area with silicified ultramafic rocks present near the thermal baths. Antimony mineralization in the northern Muratdağı region, associated with fault and fracture-controlled mineralization, was interpreted to have been formed by hydrothermal fluids during the Middle Miocene in the Göynük mine (Aral, 1989).

## GENERAL FEATURES OF Ni-LATERITES

To identify the vertical and lateral distributions of smectite and coexisting clay and non-clay minerals in the Ni-laterite deposit in the southern part of the Muratdağı, eight generalized profiles (two profiles from each locality) were prepared (Figure 2). The typical lateritic profile in the Muratdağı region displays the following zones from bottom to top: (1) harzburgitic bedrock; (2) serpentinized zone; (3) decomposed and ferruginous saprolite; and (4) Fe-S-bearing silica zone (Figures 2, 3). The saprolitic zones consist of loosely packed, lateritized materials of goethite, hematite, organic-rich smectite, and siliceous materials and enclose green to blue garnierite (Figure 3a–g). In some places, the ferruginous saprolitic zone is covered by Fe-rich silcrete (Figure 3b,c). The lateritization exhibits different zones and various mineralogical and chemical compositions. Thus, the Ni-Cr-bearing lateritic zone displays different profile distributions in different localities of the study area as outlined below.

### *Kapı Dağı locality profiles (KD)*

The laterite profiles in the Kapı Dağı locality are characterized by active, ongoing, and continuous sulfur degassing controlled by fault zones, and the local occurrence of native sulfur associated with sulfate

https://doi.org/10.1346/CCMN.2015.0630302 Published online by Cambridge University Press

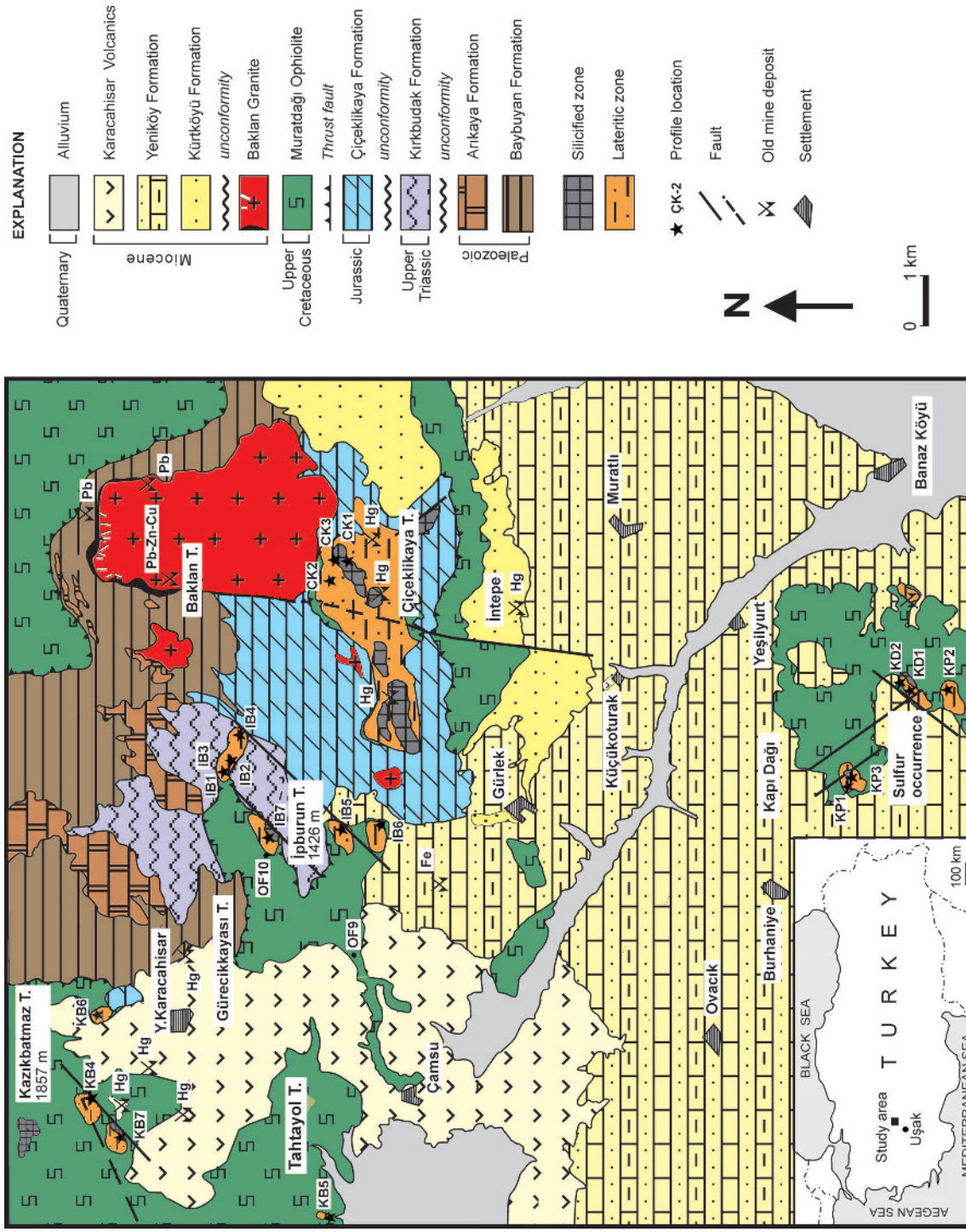


Figure 1. Geological map of the Muratdağı area (modified from Bingöl, 1977; Günay *et al.*, 1986; Aydoğan, 2006; Aydoğan *et al.*, 2008).

https://doi.org/10.1346/CCMN.2015.0630302 Published online by Cambridge University Press

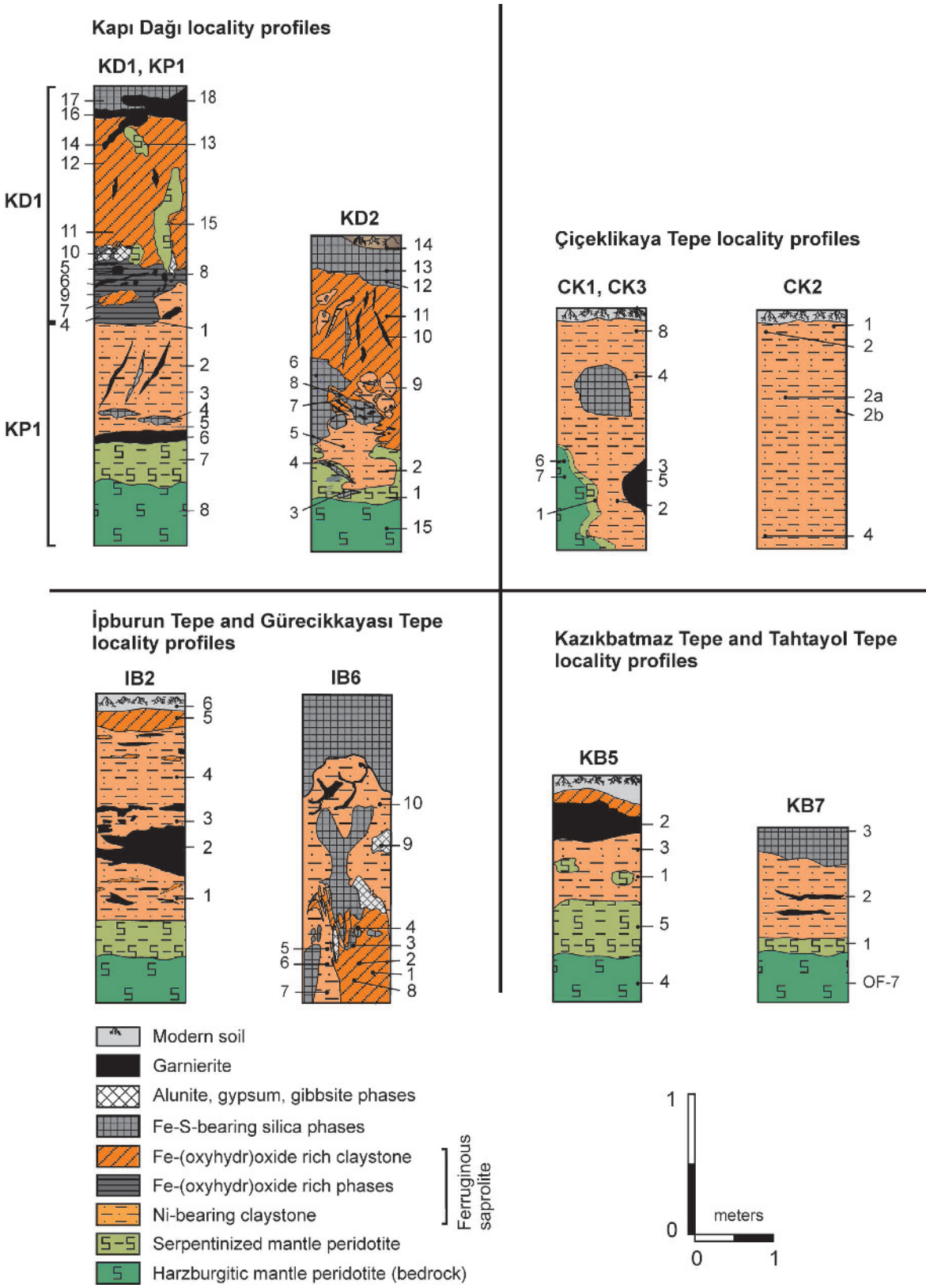


Figure 2. Schematic presentation of laterite profiles in the Muratdağı area.

https://doi.org/10.1346/CCMN.2015.0630302 Published online by Cambridge University Press

minerals. The profiles display the following zones: a zone of Ni-Cr-bearing claystone with silicified blocky serpentinites over the bedrock; a ferruginous saprolitic zone; and a zone of Fe-S-bearing silica phases at the top (Figure 3f,h). Locally, the laterite profile contains subvertical lenses of green garnierite and gypsum associated with Fe-(oxyhydr)oxide. Also present are Mn-oxide phases impregnated with gypsum, alunite, celestine, blue-colored pyrite, and marcasite along with sulfur zones. Silicification developed vertically to subvertically in fractures and fault infillings.

*Çiçeklikaya Tepe locality profiles (CK)*

This locality is dominated by Hg-rich, siliceous units with hydrothermal sources (Figure 1). Lateritization displays the following: a yellow formation within the Ni-Cr-bearing claystone; blocky silicified serpentinites; and blue-green garnierite-bearing saprolite (Figure 3a).

*İpburun Tepe and Gürecikkayası Tepe locality profiles (IB)*

This locality contains the lower level of the profiles, and consists of serpentinized ultramafics that continue upward along with a ferruginous saprolite zone dominated by Fe-(oxyhydr)oxide phases (Figures 2, 3c,e,g). Laminar and nodular garnierite is associated with the blue, brown, and yellow Fe-(oxyhydr)oxide phases in the lower level of the laterite profile. This level is overlain by Fe-(oxyhydr)oxide phases along with nodular and vein-type garnierite-bearing siliceous blocks. These profiles are covered by silcrete.

*Kazıkbatmaz Tepe and Tahtayol Tepe locality profiles (KB)*

These profiles begin with serpentinized ultramafics and continue upward with a hard, friable, asbestos-bearing serpentinized zone, garnierite-bearing ferruginous saprolite, and Fe-S-bearing silica phases (Figure 2).

## MATERIALS AND METHODS

More than 200 samples showing various degrees of chemical weathering and hydrothermal alteration were analyzed by powder X-ray diffraction (XRD) at the Turkish Petroleum Corporation (TPAO, Ankara, Turkey) using a Rigaku D/Max – 2200 Ultia PC instrument (Japan). The XRD analyses were performed with CuK$\alpha$ radiation at a scanning speed of 1º2$\theta$/min and a tube voltage and current of 40 kV and 30 mA, respectively. Samples for clay analysis (<2 μm) were prepared by separating the clay fraction by sedimentation and centrifuging the suspension after overnight dispersion in distilled water. The clay particles were dispersed by ultrasonic vibration for ~15 min. Oriented specimens of the <2 μm fractions were prepared from each sample by drying with air, solvating with ethylene glycol at 60ºC for 2 h, and treating thermally at 550ºC for 2 h. Semi-quantitative amounts of rock-forming minerals were obtained using Brindley's (1980) external standard method, whereas the relative abundances of clay-mineral fractions were determined using their basal reflections and mineral-intensity factors (Moore and Reynolds, 1989).

Scanning electron microscopy (SEM) studies were performed at the Eskişehir Osmangazi University (Turkey) using a JEOL JSM-5600LV instrument (Japan) equipped with an energy-dispersive X-ray spectroscopy (EDX) detector. Representative clay-dominated bulk samples were prepared for SEM-EDX analyses by adhering the fresh broken surface of each rock sample onto an aluminum sample holder with double-sided tape. The samples were then coated with a thin film (~350 Å) of gold using a Giko ion coater. Transmission electron microscopy (TEM) studies were carried out at the Anadolu University (Eskişehir, Turkey) using a JEOL JEM-21007 instrument. The clay particles for TEM analysis were dispersed in an ultrasonic ethanol bath for ~30 min, and one drop of each clay suspension was placed on a carbon-coated copper grid and dried at room temperature.

Thirty one samples of harzburgitic bedrock, serpentinized rock, and ferruginous saprolite were analyzed chemically for major and trace elements at Acme Analytical Laboratories Ltd. (Vancouver, Canada) using inductively coupled plasma-atomic emission spectroscopy (ICP-AES) PerkinElmer (Elan 9000) (USA). The Spectro XLAB-2000 PEDX-ray fluorescence spectrometer was calibrated using USGS standards. The ICP-AES analyses were carried out on lithium metaborate/tetraborate fusions following dilute nitric acid digestion. Loss on ignition (LOI) was determined as the weight difference after ignition at 1000ºC. The detection limits for the analyses were between 0.01 and 0.1 wt.% for major elements and between 0.1 and 5 ppm for trace elements.

The structural formulae of smectite, serpentine, and kaolinite were determined for the <2 μm clay samples with the largest smectite, serpentine, and kaolinite contents (confirmed by XRD). Separation was undertaken following the removal of free iron oxides and organic matter using the sodium dithionite-citrate procedure and hydrogen peroxide (30%) treatment, respectively (Kunze and Dixon, 1986). These samples were sieved to 2 mm; 100 g of the sieved sample was mixed with deionized water and disaggregated using a 'Stir-pak' (Cole-Parmer, UK) mixer head and mixer controller. The 2 μm fractions were subsequently isolated from the silt (2–50 μm) using repeated siphoning of the dispersed material. The clay fractions were separated by sedimentation of the suspension after 24 h of dispersion in distilled water and removal of the upper 5 cm, followed by centrifugation for 10 min at $2451 \times g$ (4000 rpm) using a Hettich Rotofix 32A centrifuge (Tuttlingen, Germany). The samples were

https://doi.org/10.1346/CCMN.2015.0630302 Published online by Cambridge University Press

then analyzed by ICP-AES at Acme Analytical Laboratories Ltd. The structural formulae of smectite, serpentine, and kaolinite were calculated on the basis of 22, 14, and 14 oxygen atoms, respectively (Moore and Reynolds, 1989).

Smectite-bearing (KD2-3, KD2-10, KB4-3), smectite+illite-bearing (KB4-6, IB2-2, IB1-7), and kaolinite-bearing (IB4-1A, IB4-1B) clay fractions representing different chemical weathering and hydrothermal conditions were chosen, purified, and analyzed for O and H stable isotopes at the Cornell Isotope Laboratory (Cornell University, New York, USA). Isotopic corrections were performed using a two-point normalization (regression) and international standards IAEA CO-1 and IAEA CO-8 for $\delta^{18}O$, and CH-7 and benzoic acid for $\delta^{2}H$. The analyses were performed using a Thermo Delta V isotope ratio mass spectrometer interfaced with a temperature-conversion elemental analyzer. The delta values for $^{18}O$ and $^{2}H$ were measured against the primary reference scale of Clayton and Mayeda (1963). The data are reported in the standard delta notation as per-mil deviations from V-SMOW (Vienna Standard Mean Ocean Water). The external reproducibility for $\delta^{18}O$ was ±0.19‰ (1σ) based on repeated analyses of an internal white crystal standard consisting of benzoic acid. The NBS 28 value was 9.61 ± 0.10‰ (1σ).

## RESULTS

### *Petrography*

The bedrock is generally composed of harzburgitic ultramafic rocks consisting of olivine, pyroxene, and minor chromite (Figure 4a). Olivine and pyroxene have been serpentinized and Fe-(oxyhydr)oxidized in serpentinized units and exhibit sieve textures locally (Figure 4b). The ferruginous saprolite zone was composed mainly of clay, Fe-(oxyhydr)oxide phases, opaque minerals, and calcite (Figures 4c–e). Opaque minerals, goethite, hematite, and pyrite, in addition to organic material were determined *via* polished-section observations.

The silcrete sample contained microcrystalline or medium- to coarse-grained quartz and some vein-like spheroidal, thin, prismatic quartz. Silicification also occurred in the form of microcrystalline quartz displaying subrounded structures coated by thin Fe-(oxyhydr)-oxide rims (Figure 4f).

### *XRD determinations*

The XRD results for the bulk samples and clay-mineral fractions taken from ophiolite-related ultramafic rocks of the Muratdağı area, showing different degrees of lateritization, indicated an abundance of smectite±illite, and local kaolinite developed by both chemical weathering and hydrothermal activity (Table 1, Figure 5). These minerals were accompanied by residual olivine and pyroxene primary bedrock minerals. Calcite and dolomite in the uppermost horizons of the laterite profiles are products of release of Ca and Mg during chemical weathering processes related to change in climate.

Locally, goethite, alunite, gypsum, pyrite, marcasite, gibbsite, celestine, barite, and native sulfur formed predominantly by hydrothermal processes operating along fault zones in the sulfur dome region were associated with the residual primary bedrock minerals olivine and pyroxene (Figures 2, 5; Table 1). In addition, smectite in laterite profiles KD and IB were impregnated with subvertical garnierite-bearing Fe-S-rich silica phases in fracture and fault infillings. As mentioned above, this suggests that smectite was produced by hydrothermal processes controlled by fault systems active since the Miocene. The degree of smectitization decreased in the Çiçeklikaya Tepe; in contrast, silicification increased. Abundant kaolinite was accompanied locally by alunite and goethite.

Smectite is generally distributed heterogeneously across most levels of the lateritic profiles (Table 1). Smectite was identified by diagnostic peaks between 15 and 16 Å, which expanded to 17–17.5 Å after ethylene-glycol treatment and collapsed to 10 Å after heating at 550ºC for 2 h (Figure 5). The $d_{060}$ value of smectite was 1.49–1.50 Å, suggesting a dioctahedral character (Moore and Reynolds, 1989). Illite was identified by peaks at 10 and 5 Å and was not affected by ethylene-glycol treatment or heating at 550ºC. The XRD backgrounds of some of the lateritized samples were slightly elevated, possibly due to the presence of amorphous and organic materials (Figure 5).

### *SEM-EDX and TEM analyses*

The SEM images indicate that flaky smectite developed in microfractures and dissolution voids by the circulation of meteoric water in the saprolitic zone (Figures 6a–f). Smectite occurred locally as a matrix between relics of olivine grains (Figure 6b). Smectite flakes with maximum dimensions of 2–10 μm occurred as regular pore- and fracture-fillings as well as grain coatings. Flaky nontronitic smectite was characterized by strong EDS peaks of Si, Al, and Fe (Figure 7a), whereas Fe-bearing montmorillonitic smectite was characterized by strong Al and Si signals along with poor Fe, Mg, Ca, and Cr signals (Figure 7b). In some places, illite fibers formed at the edge of smectite

Figure 3 (*facing page*). Field photographs showing: (a) the lateritic zone (CK); (b) garnierite covered by an Fe-bearing silica cap in a lateritic zone (KP3); (c–f) garnierite and advanced lateritization (IB1, KP3, IB2, KD1); (g) subvertical garnierite vein associated with Fe-(oxyhydr)oxide and sulfate phases (IB6); and (h) Fe-(oxyhydr)oxide phases associated with sulfate and native sulfur along a fault zone (KD1).

https://doi.org/10.1346/CCMN.2015.0630302 Published online by Cambridge University Press

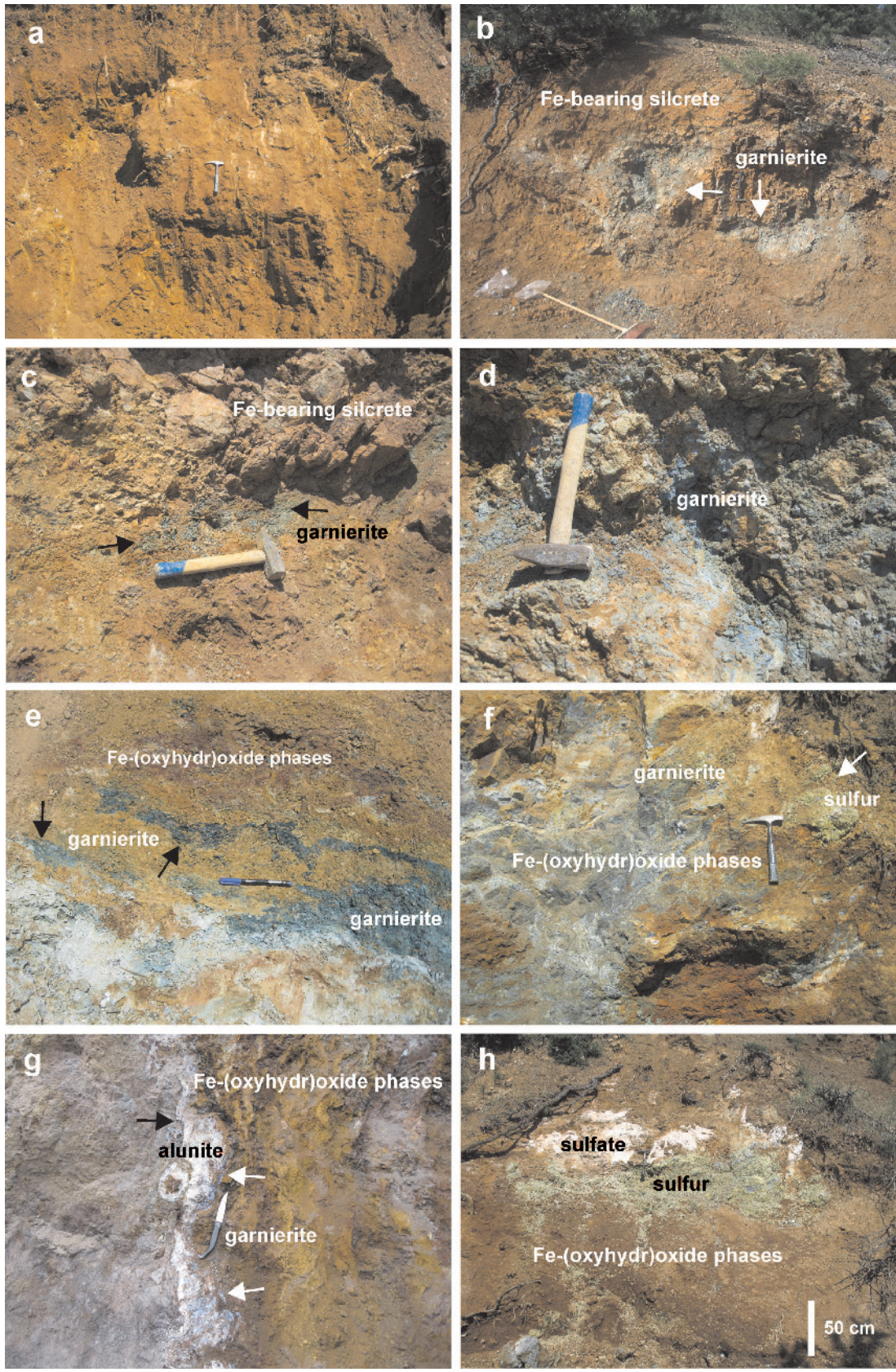


https://doi.org/10.1346/CCMN.2015.0630302 Published online by Cambridge University Press

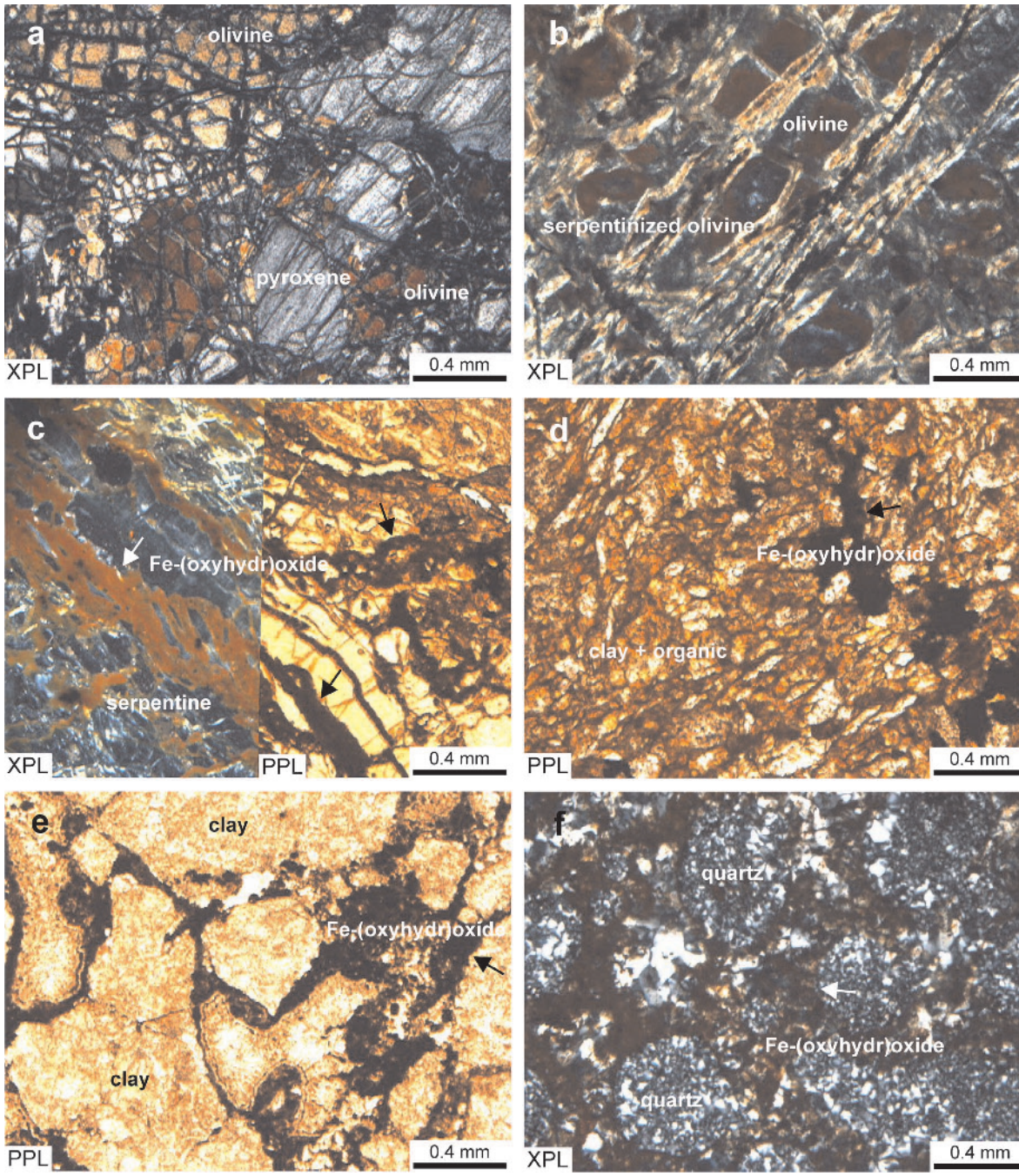


Figure 4. Photomicrographs showing: (a) olivine and pyroxene in harzburgitic bedrock (OF-5); (b) serpentinized olivine minerals displaying meshwork textures (CK5-1); (c) Fe-(oxyhydr)oxide phases in the serpentinized saprolitic zone (KD1-13); (d) clay-, Fe-(oxyhydr)oxide-, and organic-bearing ferruginous saprolitic zone (IB3-2); (e) Fe-(oxyhydr)oxide-rich infills in the fractures of ferruginous saprolite (IB1-8); and (f) microcrystalline quartz displaying subrounded forms covered by thin Fe-(oxyhydr)oxide rims (KB4-7). XPL: crossed polars; PPL: plane-polarized light.

crystals (Figures 6b,d,e). The microfracture surfaces in smectite-rich samples were covered by sub-rounded structures and mosaic-like forms resembling Fe-(oxyhydr)oxide phases, as indicated by the strong Fe peak (Figures 6f–h, 7c). Smectite crystals associated locally with lepidospheres exhibiting sub-rounded accumulations of acicular crystals yielded strong Si peaks, which are characteristic of opal-CT (Figures 6e, 7d).

Blocky alunite crystals exhibited euhedral rhombic forms with sizes of 4–10 μm (Figure 6i) and contained

https://doi.org/10.1346/CCMN.2015.0630302 Published online by Cambridge University Press

Table 1. Mineralogical variation through the profiles of lateritized ultramafic rocks.

| Sample | sme | ilt/mc | kln | srp | opl | qz | gth | alu | s | py | gp | gbs | fsp | cal | dol | ol | px |
|---|---|---|---|---|---|---|---|---|---|---|---|---|---|---|---|---|---|
| KP1-2 | ++++ | | | acc | acc | + | | | | | | | | | | | |
| KP1-3 | | + | | | | ++ | | | | | | | | + | acc | | |
| KP1-6 | +++++ | | | | | acc | | | | | | | | | | | |
| KP2-2 | | | | +++ | | | | | acc | | | | | | | ++ | |
| KP2-3 | | | | +++++ | | | | | | | | | | | | | |
| KP2-4 | +++ | | | acc | | | | | | | | | | | | + | ++ |
| KP3-4 | + | + | | +++ | | acc | | | | | | | | | | | + |
| KP3-9 | +++ | acc | | | | + | | | | | | | + | + | | | |
| KP3-10 | +++ | | | | | acc | | acc | | | | | | + | | | |
| KP3-16 | ++++ | acc | | | ++ | | | | | | | | | | | acc | + |
| KP3-18 | ++++ | + | | | acc | | | | | | | | | | | | |
| KP3-23 | ++++ | | | | + | acc | | | | | | | | | | | |
| KP3-25 | ++++ | acc | | | acc | acc | | | | | | | | | | | |
| KP3-27 | acc | | | acc | ++++ | | | | | | | | | | | | |
| KP3-28 | +++ | | ++ | | | | | | | | | | | | | | |
| KP3-29 | +++ | | | | ++ | acc | | | | | | | | | | | |
| KP3-32 | ++ | | | ++ | acc | | | | | | | | | | | | + |
| KD1-4 | + | | | | | ++++ | | | | | | | | | | | |
| KD1-5 | + | acc | | | | + | ++ | | | acc | | | | | | | |
| KD1-7 | + | + | | | | +++ | | | | | | | | | | | |
| KD1-10 | + | | | | acc | | +++ | | | | | | | | | + | |
| KD1-12 | ++ | | | | acc | | ++ | | | | | | | | | + | |
| KD1-13 | acc | | | | acc | | ++ | | | | | | | | | + | |
| KD1-17 | | acc | acc | | | acc | | | | | | ++++ | | | | | |
| KD2-1 | +++++ | | | | | acc | acc | | | | | | | | | | |
| KD2-2 | +++++ | | | | | | acc | | | | | | | | | + | |
| KD2-3 | +++++ | | | | | | + | | | | | | | | | | |
| KD2-6 | +++ | | | | | | ++ | | | | | | | | | + | |
| KD2-8 | | | | | | +++++ | | | | | | | | | | | |
| KD2-9 | +++++ | | | | | acc | | | | | | | | | | + | |
| KD2-10 | ++++ | acc | | | | + | + | | | | | | | | | | |
| KD2-12 | +++ | | | | | | ++ | | | | | | | | | + | |
| KD2-14 | ++++ | | | + | | + | acc | | | | | | | | | acc | |
| KD3-1 | | acc | | | | | | | ++++ | + | | | | | | | |
| KD3-3 | | | | | | | ++ | | +++ | | | | | | | | |
| KD3-4 | + | | | | | acc | | ++ | | | acc | + | | | acc | + | acc |
| KD3-5 | + | + | ++ | | | ++ | | | | | | | | | | | |
| CK1-1 | ++ | acc | + | | ++ | + | | | | | | | | | | | |
| CK1-8 | +++ | acc | | | ++ | + | | | | | | | | | | | |
| CK2-1 | + | acc | | | +++ | + | | | | | | | | | | | |
| CK3-1 | + | acc | | | +++ | + | | | | | | | | | | | |
| CK3-4 | + | | | | | ++++ | | | | | | | | | | | |

Table 1 (*contd.*).

| Sample | sme | ilt/mc | kln | srp | opl | qz | gth | alu | s | py | gp | gbs | fsp | cal | dol | ol | px |
|---|---|---|---|---|---|---|---|---|---|---|---|---|---|---|---|---|---|
| CK3-5 | | acc | | | +++ | + | +++++ | | | | | | | | | | |
| CKS -2 | | | | +++ | | | | | | | | | | | | ++ | ++ |
| CKS-3 | | | | +++ | | | | | | | | | | | | + | + |
| CKSL-1 | | | | + | | ++++ | | | | | | | | | | + | acc |
| CKSL-2 | | | | | | | +++++ | | | | | | | | | | |
| IB1-1 | +++ | | + | | | | acc | + | | | | | | | | + | + |
| IB1-3 | +++ | | + | | acc | | + | acc | | | | | | | | + | + |
| IB1-5 | ++ | + | acc | | | acc | + | acc | | | | | | | | | ++ |
| IB1-6 | ++++ | | + | | | | acc | acc | | | | | | | | | + |
| IB1-7 | ++++ | | + | | + | | acc | | | | | | | | | | |
| IB2-2 | +++ | acc | + | | | ++ | acc | | | | | | | | | | acc |
| IB2-4 | ++++ | acc | | | | acc | + | acc | | | | | | | | acc | |
| IB2-5 | +++ | | | | | | + | + | | | | | + | | | acc | + |
| IB2-6 | + | | | | acc | + | ++ | + | | | | | + | | | acc | acc |
| IB4-1A | | | +++++ | | | | | | | | | | | | | | |
| IB4-1B | | | +++++ | | | | | | | | | | | | | | |
| IB5-1 | ++++ | | | | + | acc | | | | | | | | | | + | |
| IB5-2 | +++ | | | | ++ | acc | | | | | | | | | | | |
| IB6-1 | +++ | acc | acc | | | acc | | ++ | | | | | | | | | |
| IB6-3 | ++ | | + | | | | ++ | + | | | | | | | | + | acc |
| IB6-4 | | | | | + | | +++ | + | | | | | | | | + | |
| IB6-5 | +++ | + | acc | | + | | | ++ | | | | | acc | | | + | acc |
| IB6-7 | | | | | + | | | | | | | | | | | + | +++ |
| IB6-9 | + | | | | | | acc | | | ++++ | | | | | | acc | |
| IB7-1 | + | | | | | ++++ | | | | | | | | | | | |
| KB7-2 | ++++ | | | | + | | | | | | | | | | | | |
| KB4-3 | +++++ | | | acc | | | | | | | + | | | | | | |
| KB4-5 | ++++ | acc | | | | | | | | | | | | | | | |
| KB4-6 | +++++ | acc | | | | | acc | | | | | | | | | | ++ |
| KB5-3 | acc | | | +++ | | | | | | | | | acc | | | | |
| KB6-6 | ++++ | | | | | acc | | | | | | | | | acc | | |
| KB7-2 | ++++ | | | | + | | | | | | | | | | | | |

sme: smectite, ilt/mc: illite/mica, kln: kaolinite, srp: serpentine, opl: opal-CT, qz: quartz, gth: goethite, alu: alunite, s: native sulfur, py: pyrite, gp: gypsum, gbs: gibbsite, fsp: feldspar, cal: calcite, dol: dolomite, ol: olivine, px: pyroxene, acc: accessory, +: relative abundance of mineral (mineral-name abbreviations after Whitney and Evans, 2010).

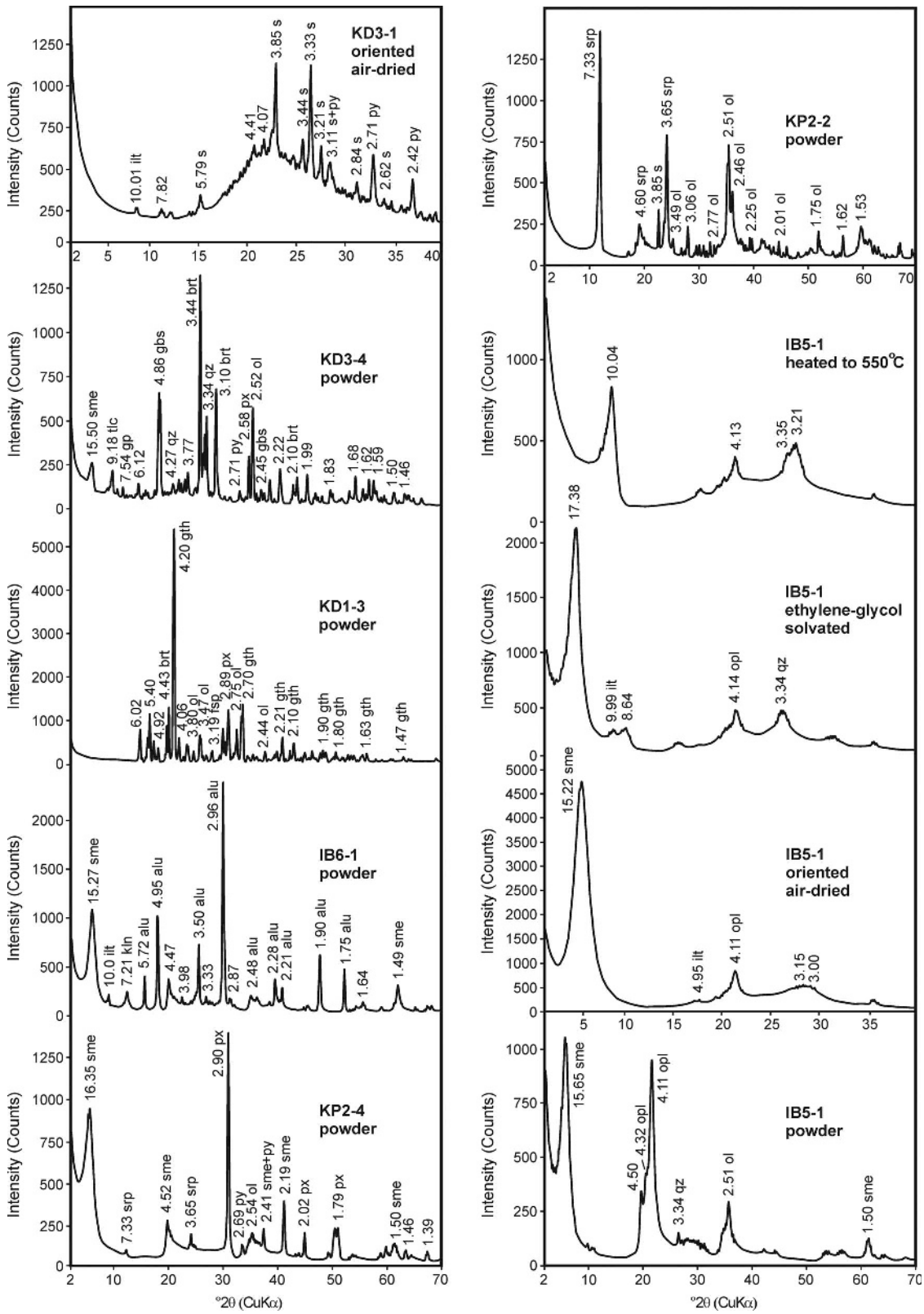


Figure 5. XRD patterns for smectite- and serpentine-dominated samples. sme: smectite, ilt: illite, kln: kaolinite, srp: serpentine, opl: opal-CT, qz: quartz, gth: goethite, alu: alunite, s: native sulfur, py: pyrite, gp: gypsum, gbs: gibbsite, brt: barite, fsp: feldspar, tlc: talc, ol: olivine, px: pyroxene (mineral-name abbreviations after Whitney and Evans, 2010).

https://doi.org/10.1346/CCMN.2015.0630302 Published online by Cambridge University Press

Al, S, and K (Figure 7e). In places, these crystals were associated with clay and the relict olivine and/or pyroxene. Blocky sulfur observed in dissolution voids consisted of rods and rod bundles of sulfur crystals associated with pyrite, gypsum, and gibbsite, which developed along fractures and dissolution voids (Figure 6j–n). Sulfur was identified based on a strong S peak; pyrite crystals exhibited strong peaks for both S and Fe, and gibbsite exhibited a strong Al peak (Figure 7e–g). Irregular structures resembling magnesium sulfate were also observed, as indicated by sharp S and Mg peaks (Figures 6o, 7h).

Kaolinite exhibited subhedral to euhedral hexagonal forms developed parallel to microfractures, which were possible micro-pathways for hydrothermal fluids (Figure 6p). The EDX spectra of kaolinite plates exhibit strong peaks for Si and Al, whereas the Fe peaks are weak (Figure 7i). Serpentine exhibited a compact, platy, and massive morphology, and enclosed surfaces showing an array of anhedral and funnel-shaped etch pits characteristic of weathered olivine (Velbel, 2009; Figure 6q,r).

The TEM images show that smectite occurred as wavy fan- and lens-like plate packets, exhibiting narrow and sharp edges resembling illite (Figure 8a–c). Kaolinite exhibited well defined hexagonal crystals with regular outlines (Figure 8d) and diameters of between 200 and 500 nm.

### *Chemical analyses*

Chemical analyses of representative harzburgitic bedrock, of serpentinized harzburgite, and of lateritized rocks (ferruginous saprolite) are given in Table 2. The chemical variations in $Al_2O_3$ (0.1–20.0 wt.%), $Fe_2O_3$ (2.9–49.8 wt.%), MgO (0.8–38.1 wt.%), and $SiO_2$ (14.8–79.0 wt.%) as well as the LOI (3.0–26.2 wt.%) reflect the mineralogies and crystal chemistries of the clay minerals that coexist with the non-clay minerals (Tables 1, 2; an extended version of Table 2 has been deposited with the Editor-in-Chief and is available for download at http://www.clays.org/JOURNAL/JournalDeposits.html). $Fe_2O_3$+$Al_2O_3$+LOI and $Fe_2O_3$ were abundant in the ferruginous saprolitic samples, corresponding to an increase in the abundances of smectite and goethite/hematite, respectively, and a decrease in the olivine and pyroxene contents compared with the bedrock samples. $Fe_2O_3$ and $Al_2O_3$ are therefore shown to be bound within the structures of nontronite, Fe-rich montmorillinite, and goethite/hematite, and increase vertically upward in the sequence of each profile, as indicated by the mineralogical determinations.

Nickel is abundant in ferruginous saprolite and in the enclosed garnierite, which were developed on serpentinized harzburgitic bedrock similar to those observed in New Caledonia (Trescases, 1975), Brazil (Barros de Oliveira *et al.*, 1992; Mano *et al.*, 2014), and Murrin Murrin, Australia (Camuti and Gifford, 1997), although garnierite is absent in the latter case. Nickel, Cr, and Co abundances increased upward through the lateritic zones relative to the harzburgitic bedrock. Nickel, Cr, and Co concentrations exhibited a positive correlation with $Fe_2O_3$ and weakly negative correlations with MgO, $Al_2O_3$, and $SiO_2$. Thus, during the saprolitization processes of ultramafics, Ni and Co are immobile, similar to Fe, in contrast to the mobile Mg and Si (Venturelli *et al.*, 1997). Locally, 69.6–82.6 wt.% of $Fe_2O_3$-bearing Fe-(oxyhydr)oxide phases contained 0.9–0.6 wt.% Ni, 2.5–0.3 wt.% $Cr_2O_3$, and 387–231 ppm Co.

### *Mineral chemistry*

The average structural formulae of nontronite, Fe-rich montmorillonite, Fe-poor montmorillonite, kaolinite, and serpentine were calculated from the chemical analyses of clay fractions (Table 3; an extended version of Table 3 has been deposited with the Editor-in-Chief and is available for download at http://www.clays.org/JOURNAL/JournalDeposits.html). The tetrahedral sites were occupied by Si, which was substituted by traces of Al and Fe in nontronite, Fe-rich montmorillonite, and serpentine, and by Al in Fe-poor montmorillonite and kaolinite. Iron was the dominant cation in the octahedral sites of nontronite and Fe-rich montmorillonite; the Fe was accompanied by Mg, Cr, Ni, and Ti in addition to Al in Fe-rich montmorillonite (Kadir and Akbulut, 2009). Magnesium was the dominant cation in the octahedral sites of serpentine and montmorillonite accompanied by Fe, Cr, Ni, Mn, and Ti. In the kaolinite, $Fe^{3+}$ substituted for some of the Al. Calcium, Na, and K were deemed to be exchangeable interlayer cations.

In the nontronite, montmorillonite, serpentine, and kaolinite crystals, Ni and Cr substituted for Fe, which was dominant in the octahedral sheets. Therefore, in lateritized units, Ni and Cr exhibited positive correla-

Figure 6 (*facing page*). SEM images of: (a) development of smectite between relict olivines in saprolite (KP3-16); (b) magnified view of smectite flakes between relict olivines (IB1-3); (c) magnified view of smectite flakes in microfractures and dissolution voids (IB6-5); (d) smectite flakes edging illite fibers (IB6-5); (e) smectite flakes edging lepidospheres and acicular crystals of opal-CT (KD1-6); (f) flaky smectite enclosing Fe-(oxyhydr)oxide phases within voids (KP3-28); (g,h) sub-rounded and mosaic-like Fe-(oxyhydr)oxide phases covering microfractures (IB6-4); (i) blocky alunite crystals (IB6-4); (j) cubic pyrite crystals (KD1-5); (k) anhedral gibbsite crystals (IB6-9); (l) blocky sulfur in dissolution voids (KD3-1); (m) rods and rod bundles of sulfur crystals associated with gypsum in microfractures (KD1-1); (n) magnified view of platy gypsum crystals (KD1-1); (o) anhedral magnesium sulfate crystals (KD1-2); (p) euhedral to subhedral kaolinite and kaolinite stacks (IB4-1A); and (q,r) compact platy serpentine bundles edging relicts of olivine (KP2-3).

https://doi.org/10.1346/CCMN.2015.0630302 Published online by Cambridge University Press

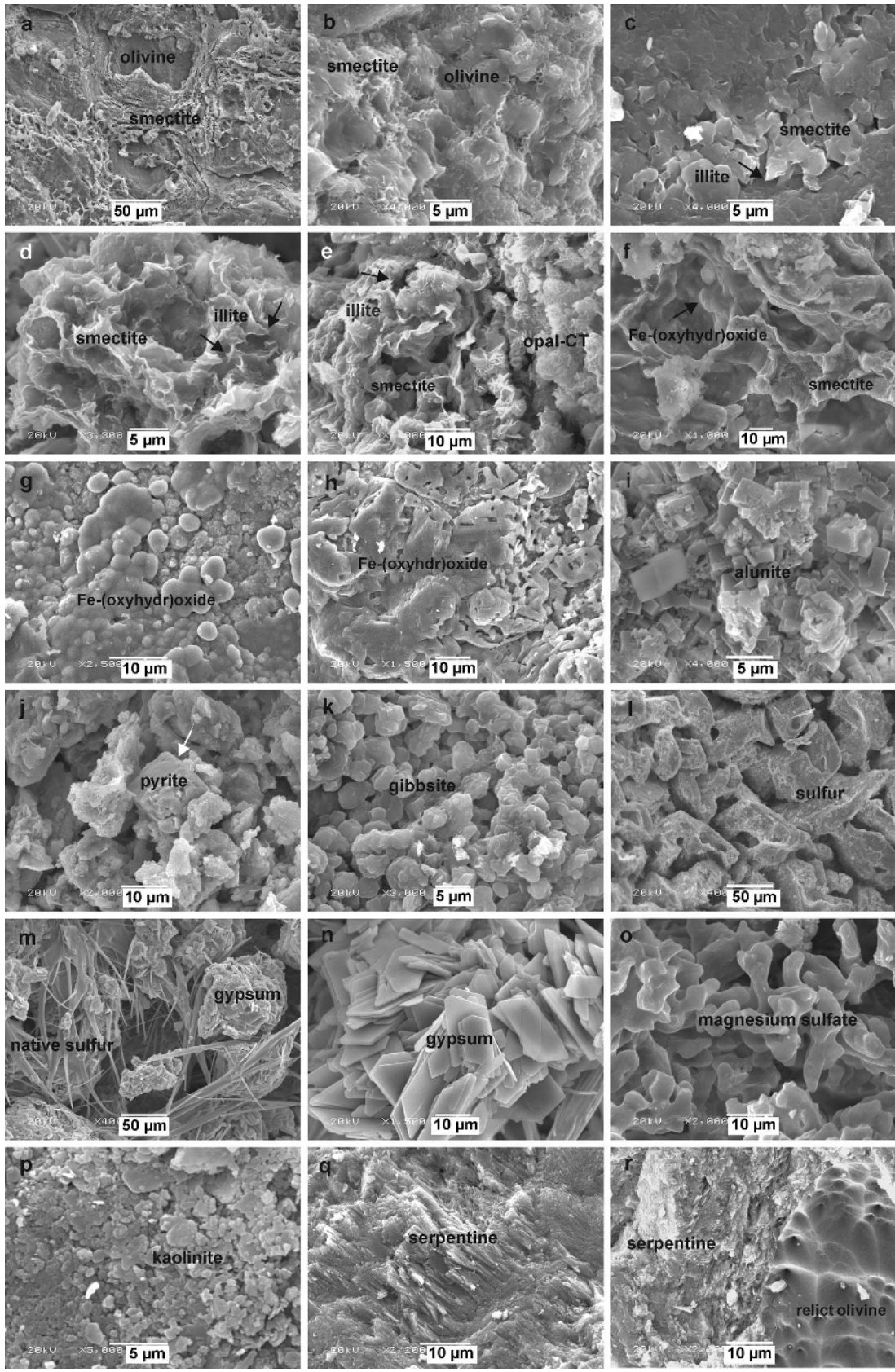


https://doi.org/10.1346/CCMN.2015.0630302 Published online by Cambridge University Press

Table 2. Major (wt.%) and trace element (ppm) compositions of various lithologies of the study area (see Table 1 for the mineralogical compositions of the samples).

| Major oxide (wt.%) | Harzburgitic bedrock avg. ($n$ = 9) | Serpentinized harzburgite avg. ($n$ = 10) | Ferruginous saprolite avg. ($n$ = 12) |
|---|---|---|---|
| $SiO_2$ | 40.8 | 43.6 | 37.5 |
| $Al_2O_3$ | 0.5 | 1.4 | 8.8 |
| $\Sigma Fe_2O_3$ | 7.9 | 13.8 | 30.6 |
| MgO | 35.9 | 21.4 | 2.6 |
| CaO | 0.5 | 3.4 | 1.8 |
| $Na_2O$ | 0.01 | 0.02 | 0.1 |
| $K_2O$ | 0.01 | 0.28 | 0.4 |
| $TiO_2$ | 0.01 | 0.06 | 0.2 |
| $P_2O_5$ | 0.01 | 0.03 | 0.1 |
| MnO | 0.11 | 0.2 | 0.1 |
| $Cr_2O_3$ | 0.4 | 0.5 | 1.7 |
| Ni | 0.2 | 0.4 | 0.6 |
| LOI | 13.0 | 14.82 | 15.3 |
| Total | 99.4 | 99.6 | 99.7 |
| TOT/C | 0.013 | 0.96 | 0.43 |
| TOT/S | 0.03 | 0.08 | 0.29 |
| Trace elements (ppm) | | | |
| Ba | 4.17 | 31.67 | 163.33 |
| Be | 1 | 1.50 | 3.14 |
| Co | 102.63 | 184.95 | 166.78 |
| Sc | 7.67 | 12.50 | 44.58 |
| Cs | 0.1 | 2.51 | 1.49 |
| Ga | 1.32 | 2.08 | 6.47 |
| Hf | 0.20 | 0.50 | 1.43 |
| Nb | 0.50 | 0.95 | 5.36 |
| Rb | 0.15 | 3.09 | 8.60 |
| Sn | 1 | 1 | 3.50 |
| Sr | 3.14 | 25.63 | 105.45 |
| Ta | 0.1 | 0.10 | 0.68 |
| Th | 0.2 | 2.25 | 12.27 |
| U | 1.40 | 1.04 | 6.76 |
| V | 34.78 | 60.60 | 253.08 |
| W | 0.60 | 1.30 | 2.47 |
| Zr | 1.22 | 4.80 | 32.89 |
| Y | 0.15 | 4.15 | 12.27 |
| Mo | 0.1 | 2.10 | 5.84 |
| Cu | 8.78 | 13.90 | 16.68 |
| Pb | 0.40 | 1.63 | 10.53 |
| Zn | 27.67 | 37.50 | 191.83 |
| Ni | 1966.83 | 63.12 | 88.26 |
| As | 2.04 | 0.30 | 0.24 |
| Cd | 0.1 | 16.05 | 4.11 |
| Sb | 0.68 | 0.1 | 0.70 |
| Bi | 0.1 | 0.80 | 0.32 |
| Ag | 0.1 | 1.63 | 5.26 |
| Au (ppb) | 1.28 | 5.34 | 13.38 |
| Hg | 0.03 | 0.65 | 4.08 |
| Tl | 0.10 | 0.80 | 1.00 |
| Se | 0.50 | 31.67 | 163.33 |

$n$: number of samples.

tions with nontronite, Fe-bearing montmorillonite, serpentine, and Fe-bearing kaolinite. The location of Ni in the Muratdağı smectite was similar to that in the smectite layers determined by Delvigne (1983) and Gaudin *et al.* (2005).

*Stable-isotope geochemistry of the smectite-dominated clay fraction*

The O- and H-isotopic compositions of the smectite, smectite+illite, and kaolinite samples are given in Table 4 and plotted in Figure 9. The $\delta^{18}O$ and $\delta D$ values ranged between −4.91‰ and +1.07‰ and between −145.03‰ and −94.94‰, respectively. The isotopic data for the smectite- and smectite+illite-dominated clay fractions in the lateritized ultramafic units fell to the right of kaolinite line in equilibrium with the meteoric waters at temperatures below 100ºC indicating low-temperature chemical weathering processes similar to those reported for the Murrin Murrin smectitic laterite profiles (Gaudin *et al*., 2005). The isotopic data for the smectite+illite, smectite, and kaolinite samples fell to the left of kaolinite line in equilibrium with the meteoric waters at temperatures above 100ºC, suggesting hydrothermally controlled processes since Miocene times (Taylor, 1974, 1979).

## DISCUSSION

Lateritic zones were observed overlying portions of the mantle peridotite in the Muratdağı area. Field observations and the mineralogical and geochemical characteristics of the lateritic profiles indicate that the complex lateritization processes were dominated mainly by surface chemical weathering-controlled alternating wet and dry periods and hydrothermal activity in four of the Kapı Dağı, Çiçeklikaya Tepe, İpburun Tepe and Gürecikkayası Tepe, and Kazıkbatmaz Tepe and Tahtayol Tepe localities (Figure 10).

Meteoric water circulated in ultramafics under humid temperate climates since the Oligocene along with fault-controlled hydrothermal fluid injection during and following the intrusion of the Miocene Baklan granite and Karacahisar volcanic activities (Gaudin *et al*., 2005; Aydoğan *et al*., 2008; Butt and Cluzel, 2013; Helvacı *et al*., 2013). Reactions with these waters resulted in the weathering and alteration of olivine and pyroxene and the release of Fe, Mg, Ni, and Cr by $H_2SO_4$ (sulfuric acid). This process is related to the surface oxidation of $H_2S$ at atmospheric pressure and different temperatures under low-pH conditions, similar to the process reported by Luo *et al.* (2009). Thus, immobile Fe±Al+Cr+Ni became enriched, whereas mobile Si and Mg were depleted (Freyssinet *et al*., 2005; Venturelli *et al*., 1997; Fan and Gerson, 2011). In contrast to the immobile behavior of Ni in the present study area, Ni, along with Si, Fe, and Mg, is mobile under acidic condition in Ni-laterite deposits in other parts of the world (Elias, 2001b; Tauler *et al*., 2009; Butt and Cluzel, 2013). These results are consistent with lateritization processes (Troly *et al.*, 1979; Brand *et al.*, 1998; Elias, 2001a, 2001b; Robb, 2004; Freyssinet *et al*.,

https://doi.org/10.1346/CCMN.2015.0630302 Published online by Cambridge University Press

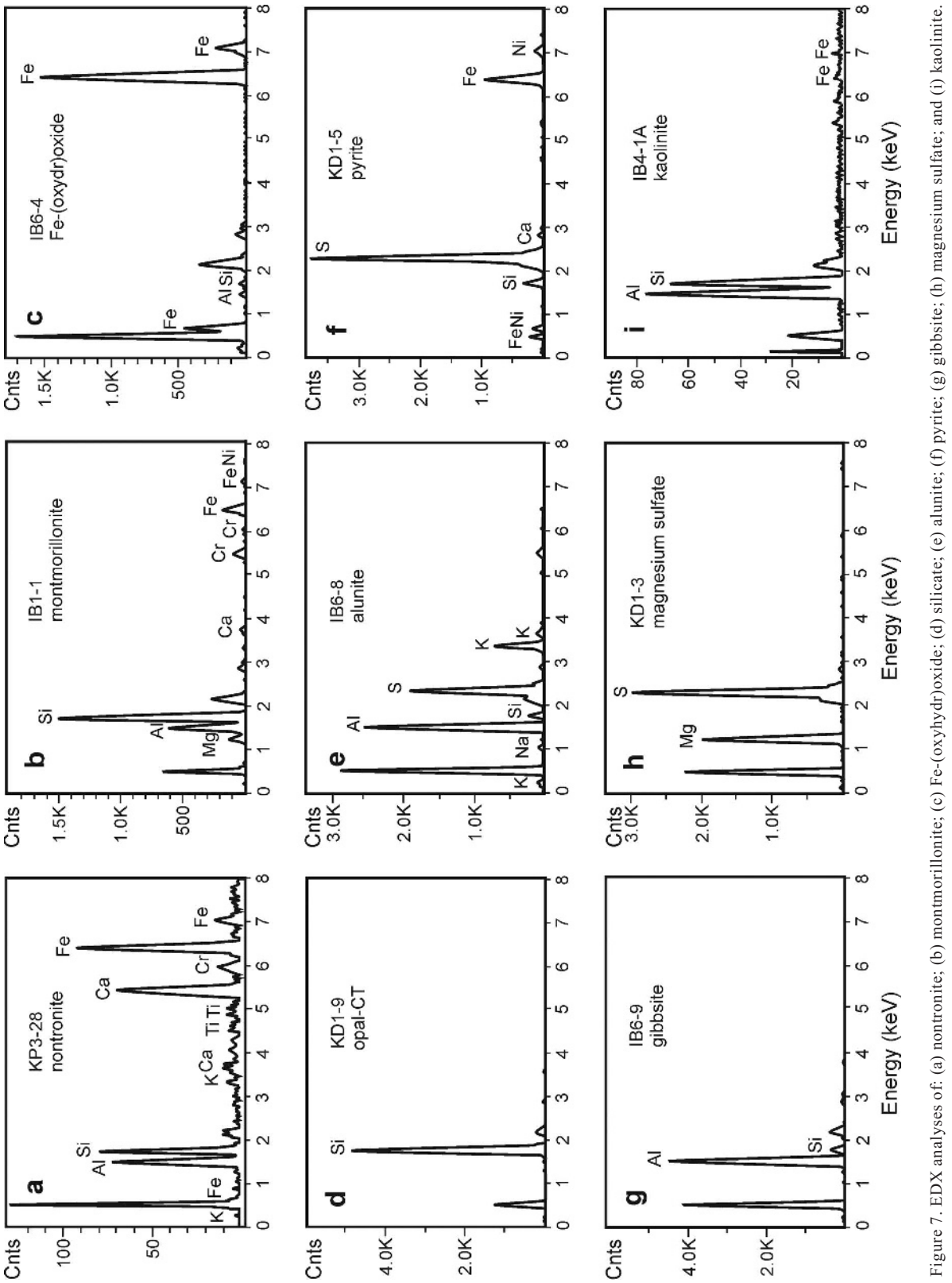


Figure 7. EDX analyses of: (a) nontronite; (b) montmorillonite; (c) Fe-(oxyhydr)oxide; (d) silicate; (e) alunite; (f) pyrite; (g) gibbsite; (h) magnesium sulfate; and (i) kaolinite.

https://doi.org/10.1346/CCMN.2015.0630302 Published online by Cambridge University Press

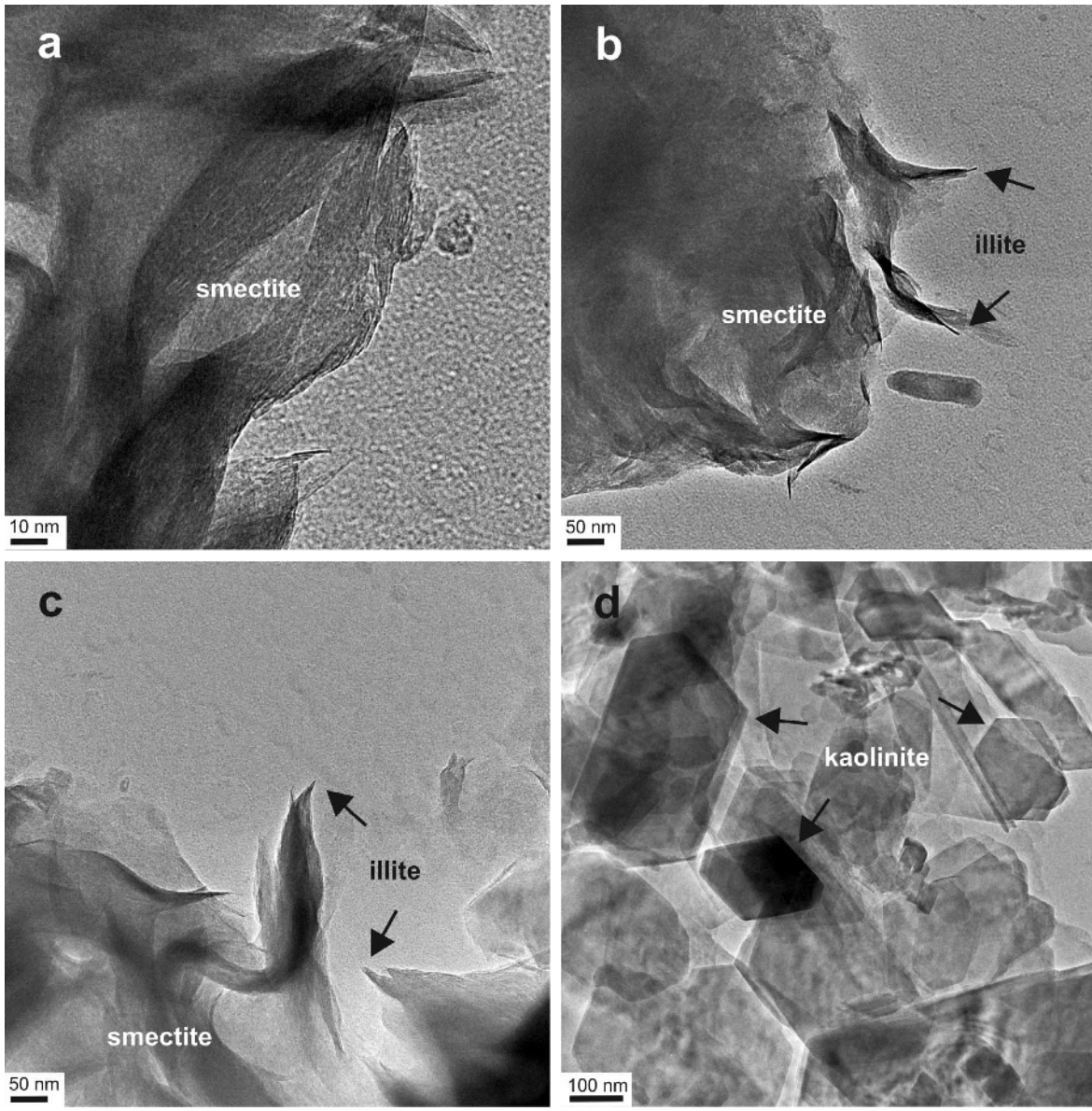


Figure 8. TEM images of: (a–c) wavy fan- and lens-like smectite plate packets edging illite fibers (KB4-3; KB4-6); and (d) hexagonal kaolinite crystals of various sizes (IB4-1A).

2005; Gaudin *et al.*, 2005). The Fe±Al and alkali contents were enriched significantly by both meteoric water and hydrothermal fluids, favoring the precipitation of abundant nontronite along with both Fe-rich and Fe-poor montmorillonites under alkaline environmental conditions (pH up to 8.5) (Berner and Berner, 1996; Meunier and Velde, 2004; Velbel and Barker, 2008; Fan and Gerson, 2011; Külah *et al.*, 2014). The Al required to precipitate montmorillonite and kaolinite originated from the fluid circulating through the chlorite-muscovite-biotite schists, granite, and volcanics in the study area (Erkoyun and Kadir, 2011; Kadir and Erkoyun, 2013). Mobility of Al is consistent with the mobile Al+Fe and immobile Si behavior in early-stage weathering mineral–water reactions in the amphibolites of the Tallulah Falls Formation in the Georgia Blue Ridge, USA (Velbel *et al.*, 2009). The local concentration of Ca resulted in calcite precipitation in pedogenic alkaline solutions in an arid environment (Kaplan *et al*., 2013; Kadir *et al.*, 2014a). Silica was released during the lateritization of ultramafic units and concentrated within fluids, resulting in the precipitation of silcrete (quartz and opal-CT) associated with Fe-(oxyhydr)oxidation.

Textural images reveal that different degrees of chemical weathering and spatially variable hydrothermal processes in ultramafic rocks resulted in the develop-

https://doi.org/10.1346/CCMN.2015.0630302 Published online by Cambridge University Press

Table 3. Chemical compositions (wt.%) and structural formulae for purified smectite, serpentine, and kaolinite samples.

| Major oxides (wt.%) | Nontronite avg. ($n$ = 3) | Fe-montmorillonite avg. ($n$ = 3) | Montmorillonite avg. ($n$ = 2) | Serpentine avg. ($n$ = 3) | Kaolinite avg. ($n$ = 4) |
|---|---|---|---|---|---|
| $SiO_2$ | 40.39 | 48.21 | 52.24 | 39.09 | 38.47 |
| $Al_2O_3$ | 3.66 | 3.67 | 14.52 | 0.8 | 33.58 |
| $\Sigma Fe_2O_3$ | 35.22 | 19.26 | 5.23 | 7.81 | 9.07 |
| MgO | 2.19 | 4.40 | 6.24 | 37.31 | 0.18 |
| CaO | 0.44 | 0.29 | 0.76 | 0.71 | 0.24 |
| $Na_2O$ | 0.06 | 0.06 | 0.16 | 0.01 | 0.06 |
| $K_2O$ | 0.14 | 0.19 | 1.49 | 0.01 | 0.19 |
| $TiO_2$ | 0.02 | 0.04 | 0.37 | 0.01 | 0.13 |
| MnO | 0.33 | 0.24 | 0.08 | 0.10 | 0.01 |
| $Cr_2O_3$ | 0.93 | 1.88 | 0.02 | 0.41 | 1.57 |
| Ni (%) | 1.15 | 1.02 | 0.18 | 0.22 | 0.03 |
| LOI | 15.07 | 16.5 | 17.60 | 12.86 | 15.30 |
| Total | 99.61 | 96.01 | 98.92 | 99.36 | 98.68 |
| $SiO_2/Al_2O_3$ | 16.95 | 13.88 | 3.60 | 50.04 | 1.15 |
| $SiO_2/R_2O_3$ | 1.08 | 2.15 | 2.65 | 4.54 | 0.93 |
| Si | 6.51 | 7.73 | 7.74 | 3.75 | 3.54 |
| Al | 0.72 | 0.21 | 0.26 | 0.09 | 0.47 |
| Fe | 0.76 | 0.05 | – | 0.16 | – |
| Σ | 8.00 | 8.00 | 8.00 | 4.00 | 4.00 |
| Al | – | 0.48 | 2.28 | – | 3.24 |
| Fe | 3.57 | 2.25 | 0.58 | 0.42 | 0.66 |
| Mg | 0.53 | 1.04 | 1.38 | 5.34 | 0.03 |
| Ti | 0.003 | 0.005 | 0.04 | 0.001 | 0.01 |
| Mn | 0.06 | 0.04 | 0.02 | 0.01 | 0.001 |
| Cr | 0.20 | 0.38 | 0.004 | 0.05 | 0.18 |
| Ni | 0.40 | 0.27 | 0.07 | 0.03 | 0.006 |
| Σ | 4.76 | 4.47 | 4.37 | 5.85 | 4.13 |
| Ca | 0.07 | 0.05 | 0.12 | 0.07 | 0.02 |
| Na | 0.02 | 0.02 | 0.05 | 0.002 | 0.01 |
| K | 0.03 | 0.04 | 0.29 | 0.001 | 0.04 |
| Σ | 0.12 | 0.11 | 0.45 | 0.07 | 0.05 |
| Tetrahedral charge | 1.50 | 0.24 | −0.26 | 0.25 | −0.43 |
| Octahedral charge | 1.29 | 0.11 | −0.31 | 0.14 | 0.35 |
| Total charge | 0.21 | 0.18 | 0.57 | 0.15 | −0.09 |
| Interlayer charge | 0.21 | 0.16 | 0.56 | 0.15 | −0.08 |
| $x_t/x_o$ | 1.30 | 1.86 | 0.81 | 5.37 | −1.57 |

$x_t/x_o$: tetrahedral charge/octahedral charge ratio.
$n$: number of samples.

Table 4. Oxygen- and hydrogen-isotopic compositions of clay minerals from the lateritized ultramafic rocks.

| Sample ID | Mineralogy | Weight (mg) | %H | Normalized $\delta^2H$ *vs.* VSMOW | %O | Normalized $\delta^{18}O$ *vs.* VSMOW |
|---|---|---|---|---|---|---|
| KB4-3 | Smectite | 0.808 | 1.57 | −95.94 | 13.28 | −1.44 |
| KD2-3 | Smectite | 0.818 | 0.70 | −136.98 | 6.91 | 1.07 |
| KD2-10 | Smectite | 0.805 | 0.84 | −145.03 | 8.57 | −2.14 |
| IB1-7 | Smectite+illite | 0.798 | 1.25 | −136.45 | 10.57 | −4.91 |
| IB2-2 | Smectite+illite | 0.786 | 1.21 | −121.83 | 10.21 | −0.90 |
| KB4-6 | Smectite+illite | 0.814 | 1.27 | −107.11 | 9.67 | −1.99 |
| IB4-1B | Kaolinite | 0.757 | 1.62 | −100.88 | 13.18 | −0.09 |
| IB4-1A | Kaolinite | 0.832 | 1.55 | −100.83 | 12.08 | −0.76 |

https://doi.org/10.1346/CCMN.2015.0630302 Published online by Cambridge University Press

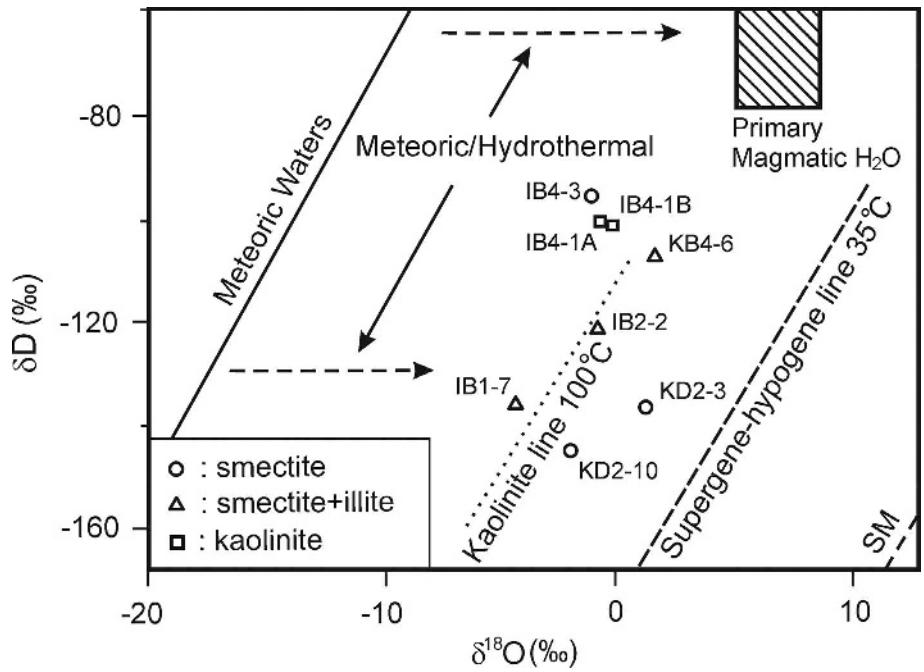


Figure 9. δD *vs.* $\delta^{18}O$ plot displaying the isotopic compositions of smectite, smectite+illite, and kaolinite from the study area. The kaolinite lines indicate equilibrium with meteoric water at temperatures of 100ºC (Hayba *et al*., 1985). The supergene/hypogene line of kaolinite equilibrium with meteoric water at 35ºC is from Sheppard *et al.* (1969). The smectite line (SM) representing the isotopic composition in equilibrium with meteoric water at 20ºC is from Savin and Epstein (1970). The meteoric water line is from Craig (1961).

ment of various Fe-(oxyhydr)oxide phases as lenses and veins with silicification and carbonatization within the lateritic zone. Micromorphological images show that smectite and smectite±illite developed as dense flake masses in dissolution voids and microfractures; this distribution suggests that the smectite had precipitated from dissolved materials in solution as well as by direct replacement of olivine and/or pyroxene (Velbel and Barker, 2008). The formation of sub-rounded and mosaic-like iron structures on the surface of microfractures, the occurrence of both garnierite and Fe-(oxyhydr)oxide phases as fracture infill, and layers within lateritized ultramafic units along with their reddish-brownish coloration due to Fe-(oxyhydr)oxides also support the proposed saprolitization and hydrothermal activities (Helvacı *et al.*, 2013; Eren *et al.*, 2015). Changes in Fe-(oxyhydr)oxide concentrations associated with silicification and S-bearing phases along the KD1 and IB6 profiles and Fe-rich silicification in fracture and fault infillings in the Kazıkbatmaz Tepe, Çiçeklikaya Tepe, and Kapı Dağı localities, reveal development through several different phases of hydrothermal activity during or following chemical weathering processes. Thus, periodic changes and acidic (pH 3−3.5) hydrothermal activity resulted in the enrichment of S, Ni, and Co, which have immobile character, Fe, Al, and K during several phases. This process resulted in the precipitation of black and dark-gray pyrite, marcasite, goethite, and yellow native sulfur crystals in an anaerobic, reducing environment in some intervals along with some local occurrences of alunite and Mg sulfate associated with garnierite and Fe-(oxyhydr)oxide phases (*e.g.* KD1; Schwertmann, 1993; Kämpf *et al.*, 2000). The continuous on-going degassing of S through fault zones favored the precipitation of native sulfur crystals, and the development of sulfur domes in the Kapı Dağı locality also support the suggestion of present-day hydrothermal activity affecting and modifying saprolite. The local association of S with Al+Fe and K resulted in the formation of alunite (Mutlu *et al.*, 2006; Ece and Schroeder, 2007; Ece *et al*., 2008). The concentration of $Fe_2O_3$ (49.7%) in sample IB1-5, Ba (1208 ppm) in sample KD2-8, and S (24.8%), Hg (39.12 ppm), Ar (630 ppm), and Co (293 ppm) in sample KD1-4 were due to a hydrothermal process presumably related to the intrusion of the Miocene Baklan granite (Nagasawa, 1978; Inoue, 1995; Aydoğan *et al*., 2008).

Nickel and Cr were positively correlated with the Fe content in the nontronite and Fe-bearing montmorillonite structures (Table 3) along with Fe-(oxyhydr)oxide phases (*e.g.* samples CKSL-2 and IB6-4; Table 2). Thus, Ni-Cr-bearing nontronite and montmorillonite precipitated from alkaline water rich in Fe and poor in Al and Mg under the control of both chemical weathering and hydrothermal processes. The relative increase of Ni+Cr in ultramafic rocks along with their positive correlation with Fe and the coexistence of smectite in lateritized ultramafic rocks revealed that the chemical weathering and hydrothermal

https://doi.org/10.1346/CCMN.2015.0630302 Published online by Cambridge University Press

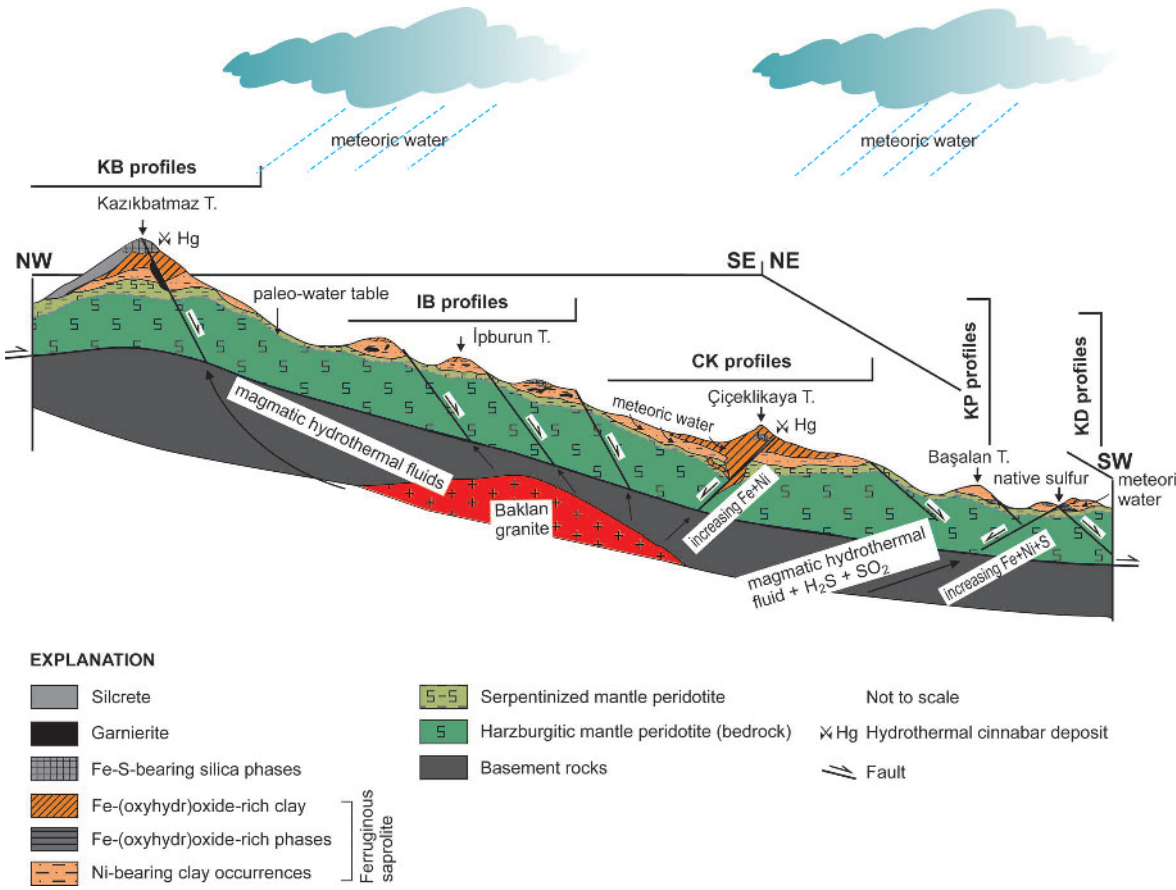


Figure 10. Genetic model for laterization processes in the Muratdağı region.

dissolution processes of olivine and pyroxene in the basement units were an important source of elements required for the formation of smectite and were controlled by basic environmental conditions.

The $\delta^{18}O$ and $\delta D$ values for pure smectite, smectite+illite, and kaolinite sample fractions plot between the supergene/hypogene line in equilibrium with meteoric water at 35ºC and meteoric and primary magmatic water, and the variability in these values may indicate that smectite formed from meteoric waters with a composition developed under a chemical weathering-related process that was controlled by climatic conditions (Gaudin *et al*., 2005; Figure 9). In addition, smectite+illite and kaolinite formed by hydrothermal activities along tectonically controlled zones (Figure 10). This interpretation is also supported by the local association of alunite and pyrite with garnierite-bearing saprolite along fault zones, which indicates a local increase in temperature in the range 70−340ºC (Deyell and Dipple, 2005; Kadir *et al*., 2014b).

## CONCLUSION

Large-scale, complex, and heterogeneous lateritization developed on harzburgitic ultramafic units in the southern part of the Muratdağı region. Olivine and pyroxene in lateritized harzburgitic bedrock were weathered by circulation of acid meteoric water under humid conditions since the Oligocene, resulting in the development of the ferruginous saprolitic zone. Subsequently, Fe and Ni+Cr were enriched, Al was slightly enriched, and Mg+Si was depleted, resulting in the precipitation of nontronite and Fe-bearing montmorillonite associated with Fe-(oxyhydr)oxide phases in saprolite from alkaline water under the control of both chemical weathering (related to changes in climate which probably started in the Oligocene) and hydrothermal activity along faults since the Miocene.

The multicolored, Fe-rich saprolite and serpentinized ultramafics reflect the fluctuation between reducing and oxidizing conditions in the lateritization environment. The association of the Fe-rich silica zone with gypsum and alunite and the infilling of fractures and faults by local native sulfur were controlled tectonically by hydrothermal processes related to granitic intrusion and volcanic activities in the region.

Nickel was concentrated in nontronitic smectite associated with an increase in the amount of Fe in the crystal structures of the ferruginous saprolitic zone. Field observations along with mineralogical and geo-

https://doi.org/10.1346/CCMN.2015.0630302 Published online by Cambridge University Press

chemical investigations of Ni deposits in the Muratdağı area suggest dominant Type B and local Type C formation models. Thus, Fe and Mg (associated with Ni and Cr) required for the formation of smectite were supplied by lateritized ultramafic rocks, whereas Al was supplied by schist, granite, and volcanic units.

The data and formation model of the Muratdağı nickel laterite deposit provide significant information on the complex influence of both paleoclimatic chemical weathering and tectonically controlled hydrothermal processes on ultramafic units; the latter factor has been recognized rarely in nature.

## ACKNOWLEDGMENTS

This present study was supported financially by the Scientific and Technological Research Council of Turkey (TUBITAK) in the framework of Project 110Y306. The authors are indebted to the anonymous reviewers, to the Editor in Chief, Michael A. Velbel, and to the Managing Editor, Kevin Murphy, for their extremely careful and constructive reviews which improved the quality of the paper significantly. Tacit Külah and Nergis Önalgil are also thanked for their assistance during the drafting of the figures and calculation of the structural formulae of the clay minerals, respectively. This paper was presented at the 50th Anniversary Annual Meeting of The Clay Minerals Society, University of Illinois at Urbana-Champaign, Illinois, USA, 2013.

## REFERENCES

Alcock, R.A. (1988) The character and resources available to the nickel industry. Pp. 67–89 in: *Extractive Metallurgy of Nickel and Cobalt* (C.P. Tyroler and C.A. Landolt, editors). The Metallurgical Society, 117th TMS Annual Meeting Proceedings, Phoenix, Arizona, USA.

Aral, H. (1989) Antimony mineralization in the northern Muratdağı (western Turkey). *Economic Geology*, **84**, 780–787.

Aydoğan, M.S. (2006) Baklan Graniti (Muratdağı, Banaz/Uşak) civarındaki baz metal cevherleşmesinin mineral parajenezi, metal zonlanması ve kökenlerinin izotop jeokimyası ile saptanması. Doktora Tezi, Süleyman Demirel Üniversitesi, Fen Bilimleri Enstitüsü, 238 s.

Aydoğan, M.S., Çoban, H., Bozcu, M., and Akıncı, Ö. (2008) Geochemical and mantle-like isotopic (Nd, Sr) composition of the Baklan Granite from the Muratdağı Region (Banaz, Uşak), western Turkey: Implications for input of juvenile magmas in the source domains of western Anatolia Eocene-Miocene granites. *Journal of Asian Earth Sciences*, **33**, 155–176.

Barros de Oliveira, S.M., Trescases, J.J., and José Melfi, A. (1992) Lateritic nickel deposits of Brazil. *Mineralium Deposita*, **27**, 137–146.

Başarı, N. (1982) Uşak, Banaz, Kızılcaören Köyü Demir – Manganez Cevreleşmesi Jeoloji Raporu. MTA Report No. 7182.

Berner, E.K. and Berner, R.A. (1996) *Global Environment: Water, Air, and Geochemical Cycles*, Princeton University Press, New Jersey, USA, 376 pp.

Bingöl, E. (1977) Muratdağı jeolojisi ve ana kayaç birimlerinin petrolojisi. *Türkiye Jeoloji Kurumu Bülteni*, **20**, 13–66.

Brand, N.W., Butt, C.R.M., and Elias, M. (1998) Nickel laterites: classification and features. *AGSO Journal of Australian Geology and Geophysics*, **17**, 81–88.

Brindley, G.W. (1980) Quantitative X-ray analysis of clays. Pp. 411–438 in: *Crystal Structures of Clay Minerals and their X-ray Identification* (G.W. Brindley and G. Brown, editors). Mineralogical Society Monograph **5**, London.

Brindley, G.W. and Maksimovic, Z. (1974) The nature and nomenclature of hydrous nickel-containing silicates. *Clay Minerals*, **10**, 271–277.

Brindley, G.W., Bish, D., and Wan, H.M. (1979) Compositions, structures, and properties of nickel-containing minerals in the kerolite–pimelite series. *American Mineralogist*, **64**, 615–625.

Butt, C.R.M. and Cluzel, D. (2013) Nickel laterite ore deposits: weathered serpentinites. *Elements*, **9**, 123–128.

Çağatay, A., Altun, Y., and Arman, B. (1981) Çaldağ (Manisa-Turgutlu) Lateritik Demir, Nikel-Kobalt Yatağının Mineralojisi. *MTA Dergisi*, 124–139.

Camuti, K.S. and Gifford, M.G. (1997) Mineralogy of the Murrin Murrin nickel laterite deposit, western Australia. Pp. 407–410 in: *Mineral Deposits* (H. Papunan, editor). A.A. Balkema, Rotterdam.

Christidis, E.G. and Mitsis, I. (2006) A new Ni-rich stevensite from the ophiolite complex of Orthrys, central Greece. *Clays and Clay Minerals*, **54**, 653–666.

Clayton, R.N. and Mayeda, T.K. (1963) The use of bromine pentafluoride in the extraction of oxygen from oxides and silicates for isotopic analysis. *Geochimica et Cosmochimica Acta*, **27**, 43–52.

Çolakoğlu, A.R. (2009) Geochemical and mineralogical characteristics of Fe-Ni laterite ore of Sarıçimen (Çaldıran-Van) Area in Eastern Anatolia, Turkey. *Turkish Journal of Earth Sciences*, **18**, 449–464.

Cornwall, H.R. (1966) Nickel Deposits of North America. *United States Geological Survey Bulletin*, **1223**, 62 pp.

Craig, H. (1961) Isotopic variations in meteoric waters. *Science*, **133**, 1702–1703.

Decarreau, A., Colin, F., Herbillon, A., Manceau, A., Nahon, D., Paquet, H., Trauth-Badaud, D., and Trescases, J.J. (1987) Domain segregation in Ni-Fe-Mg-smectites. *Clays and Clay Minerals*, **35**, 1–10.

Delvigne, J. (1983) Micromorphology of the alteration and weathering of pyroxenes in the Koua Bocca ultramafic intrusion, Ivory Coast, West Africa. Pp. 57–68 in: *Pétrologie des Altérations et des Sols, Volume II* (D. Nahon and Y. Noack, editors). Sciences Géologiques, Mémoires, vol. **72**, Strasbourg, France.

Deyell, C.L. and Dipple, G.M. (2005) Equilibrium mineral-fluid calculations and their application to the solid solution between alunite and natroalunite in the El Indio-Pascua belt of Chile and Argentina. *Chemical Geology*, **215**, 219–234.

Ece, Ö.I. and Schroeder, P.A. (2007) Clay mineralogy and chemistry of halloysite and alunite deposits in the Turplu area, Balıkesir, Turkey. *Clays and Clay Minerals*, **55**, 18–35.

Ece, Ö.I., Schroeder, P.A., Smilley, M., and Wampler, M. (2008) Acid-sulfate alteration of volcanic rocks and genesis of halloysite and alunite deposits in the Biga Peninsula, NW Turkey. *Clay Minerals*, **43**, 281–315.

Elias, M., Donaldson, M.J., and Giorgetta, N. (1981) Geology, mineralogy and chemistry of nickel cobalt deposit, near Kalgoorlie, western Australia. *Economic Geology*, **76**, 1175–1783.

Elias, M. (2001a) Global laterite resources. *Australian Journal of Mining*, **16**, 64–65.

Elias, M. (2001b) Nickel laterite deposits – geological overview, resources and exploitation. *Giant Ore Deposit: Characteristics, Genesis and Exploration*, 205–220.

Eren, M., Kadir, S., Kapur, S., Huggett, J., and Zucca, C. (2015) Colour origin of Tortonian red mudstones within the Mersin area, southern Turkey. *Sedimentary Geology*, **318**, 10–19.

Ersoy, Y. and Helvacı, C. (2007) Stratigraphy and geochemical features of the Early Miocene bimodal (ultrapotassic and calc-alkaline) volcanic activity within the NE-trending Selendi Basin, western Anatolia, Turkey. *Turkish Journal of Earth Sciences*, **16**, 117–139.

Ersoy, E.Y., Helvacı, C., and Palmer, M.R. (2011) Stratigraphic, structural and geochemical features of the NE–SW trending Neogene volcano-sedimentary basins in western Anatolia: Implication for associations of supra-detachment and transtensional strike-slip basin formation in extensional tectonic setting. *Journal of Asian Earth Sciences*, **41**, 159–183.

Ersoy, Y.E., Çemen, İ., Helvacı, C., and Billor, Z. (2014) Tectono-stratigraphy of the Neogene basins in Western Turkey: Implications for tectonic evolution of the Aegean Extended Region. *Tectonophysics*, **635**, 33–58.

Erkoyun, H. and Kadir, S. (2011) Mineralogy, micromorphology, geochemistry and genesis of a hydrothermal kaolinite deposit and altered Miocene host volcanites in the Hallaçlar area, Uşak, western Turkey. *Clay Minerals*, **46**, 421–448.

Fan, R. and Gerson, A.R. (2011) Nickel geochemistry of a Philippine laterite examined by bulk and microprobe analyses. *Geochimica et Cosmochimica Acta*, **75**, 6400–6415.

Freyssinet, P., Butt, C.R.M., Morris, R.C., and Piantone, P. (2005) Ore-forming processes related to lateritic weathering, in *Economic Geology* 100th Anniversary Volume, p. 681–722, Appendix (CD) 7 pp.

Gaudin, A., Decarreau, A., Noack, Y., and Grauby, O. (2005) Clay mineralogy of the nickel laterite ore developed from serpentinised peridotites at Murrin Murrin, Western Australia. *Australian Journal of Earth Sciences*, **52**, 231–241.

Gleeson, S.A., Butt, C.R.M., and Elias, M. (2003) Nickel laterites: A review. *Society of Economic Geologists Newsletter*, **54**, 10–16.

Gleeson, S.A., Herrington, R.J., Durango, J., and Velázquez, C.A. (2004) The mineralogy and geochemistry of the Cerro Matoso S.A. Nickel laterite deposit, Montelbano, Colombia. *Economic Geology*, **99**, 1197–1213.

Gökçe, A. (1987) Geology of the antimony mineralization in the Muratdağı (Gediz-Kütahya) region. *Bulletin of the Faculty of Engineering, Cumhuriyet University*, **4**, 65–85.

Gökçe, A. and Spiro, B. (1994) Stable isotope study of antimony deposits in the Muratdağı region, western Turkey. *Mineralium Deposita*, **29**, 361–365.

Günay, E., Akdeniz, N., Şaroğlu, F., and Çağlayan, A. (1986) Muratdağı-Gediz dolayının jeolojisi. Maden Tetkik ve Arama Genel Müdürlüğü Rapor No: 8046. Ankara (yayımlanmamış) (in Turkish).

Hayba, D.O., Bethke, P.M., Heald, P., and Faley, N.K. (1985) Geologic, mineralogic and geochemical characteristics of volcanic-hosted epithermal precious-metal deposits. *Reviews in Economic Geology*, **2**, 129–167.

Helvacı, C., Gündoğan, İ., Oyman, İ., Sözbilir, H., and Parlak, O. (2007) Çaldağ (Turgutlu-Manisa) lateritik Ni-Co yatağının jeolojisi, mineralojisi ve jeokimyasal özellikleri. Çukurova Üniversitesi Jeoloji Mühendisliği Bölümü. 30. yıl Jeoloji Sempozyumu, Adana, pp. 46–48.

Helvacı, C., Gündoğan, İ., Oyman, T., Sözbilir, H., and Parlak, O. (2008) Çaldağ (Turgutlu-Manisa) lateritik Ni-Co yatağının jeolojisi, mineralojisi, jeokimyası ve oluşum modeli. Türkiye Bilimsel ve Teknik Araştırma Kurumu Proje No: ÇAYDAĞ/104Y337, 176 pp (in Turkish).

Helvacı, C.,Gündoğan, İ., Oyman, T., Sözbilir, H., and Parlak, O. (2013) Çaldağ (Turgutlu-Manisa) Lateritik Ni-Co Yatağının Jeolojisi, Mineralojisi ve Jeokimyasal Özellikleri. *Yerbilimleri*, **34**, 101–132.

Inoue, A. (1995) Formation of clay minerals in hydrothermal environments. Pp. 268–329 in: *Origin and Mineralogy of Clays: Clays and the Environment* (B. Velde, editor). Springer-Verlag, Berlin.

Kadir, S. and Akbulut, A. (2009) Mineralogy, geochemistry and genesis of the Taşoluk kaolinite deposits in pre-Early Cambrian metamorphites and Neogene volcanites of Afyonkarahisar, Turkey. *Clay Minerals*, **44**, 89–112.

Kadir, S. and Erkoyun, H. (2013) Genesis of the hydrothermal Karaçayır kaolinite deposit in Miocene volcanics and Palaeozoic metamorphic rocks of the Uşak-Güre basin, western Turkey. *Turkish Journal of Earth Sciences*, **22**, 444–468.

Kadir, S., Eren, M., Külah, T., Önalgil, N., Cesur, M., and Gürel, A. (2014a) Genesis of Late Miocene-Pliocene lacustrine palygorskite and calcretes from Kırşehir, central Anatolia, Turkey. *Clay Minerals*, **49**, 473–494.

Kadir, S., Külah, T., Eren, M., Önalgil, N., and Gürel, A. (2014b) Mineralogical and geochemical characteristics and genesis of the Güzelyurt alunite-bearing kaolinite deposit within the Late Miocene Gördeles ignimbrite, central Anatolia, Turkey. *Clays and Clay Minerals*, **62**, 477–599.

Kämpf, N., Scheinost, A.C., and Schulze, D.G. (2000) Oxide minerals. Pp. 125–168 in: *Handbook of Soil Science* (M.E. Sumner, editor). CRC Press, Boca Raton, Florida.

Kaplan, M.Y., Eren, M., Kadir, S., and Kapur, S. (2013) Mineralogical, geochemical and isotopic characteristics of Quaternary calcretes in the Adana region, southern Turkey: Implications on their origin. *Catena*, **101**, 164–177.

Karaoğlu, Ö. and Helvacı, C. (2012) Growth, destruction and resurgence of three volcanic centers in the Miocene Uşak-Güre basin, western Turkey: subaqueous-subaerial volcanism in a lacustrine setting. *Journal of Volcanology and Geothermal Research*, **245–246**, 1–20.

Karaoğlu, Ö., Helvacı, C., and Ersoy, E.Y. (2010) Petrogenenesis and Ar-40/Ar-39 geochronology of the volcanic rocks of the Uşak-Güre basin, western Turkey. *Lithos*, **119**, 193–210.

Külah, T., Kadir, K., Gürel, A., Eren, M., and Önalgil, N. (2014) Mineralogy, geochemistry, and genesis of mudstones in the Upper Miocene Mustafapaşa member of the Ürgüp formation in the Cappadocia region, central Anatolia, Turkey. *Clays and Clay Minerals*, **62**, 267–285.

Kunze, G.W. and Dixon, J.B. (1986) Pretreatment for mineralogical analysis. Pp. 91–99 in: *Methods of Soil Analysis, Part 1, Physical and Mineralogical Methods* (A. Klute, editor). Soil Science Society of America, Madison, Wisconsin, USA.

Luo, W., Feng, Q., Ou, L., Zhang, G., and Lu, Y. (2009) Fast dissolution of nickel from a lizardite-rich saprolitic laterite by sulphuric acid at atmospheric pressure. *Hydrometallurgy*, **96**, 171–175.

Mano, E.S., Caner, L., Petit, S., Chaves, A.P., and Mexias, A.S. (2014) Mineralogical characterization of Ni-bearing smectites from Niquelândia, Brazil. *Clays and Clay Minerals*, **62**, 324–335.

Meunier, A. and Velde, B. (2004) *Illite, Origin, Evolution and Metamorphism*. Springer-Verlag Berlin Heidelberg New York, 286 pp.

Moore, D.M. and Reynolds, R.C. (1989) *X-ray Diffraction and the Identification and Analysis of Clay Minerals*. Oxford University Press, New York, 332 pp.

Mutlu, H., Sarıiz, K., and Kadir, S. (2006) Geochemistry and origin of the Şaphane alunite deposit, western Anatolia, Turkey. *Ore Geology Review*, **26**, 39–50.

Nahon, D.B. and Colin F. (1982) Chemical weathering of orthopyroxenes under lateritic conditions. *American Journal of Sciences*, **282**, 1232–1243.

Nagasawa, K. (1978) Kaolin minerals. Pp. 189–219 in: *Clays and Clay Minerals of Japan* (T. Sudo and S. Shimoda,

editors). Developments in Sedimentology, **26**, Elsevier, Tokyo.

Öner, Z. and Dilek, Y. (1999) Supradetachment basin evolution during continental extension: The Aegean province of western Anatolia, Turkey. *Geological Society of America Bulletin*, **123**, 2115–2141.

Robb, L. (2004) *Introduction to Ore Forming Processes*. Wiley-Blackwell, Oxford, 384 pp.

Savin, S.M. and Epstein, S. (1970) The oxygen and hydrogen isotope geochemistry of clay minerals. *Geochimica et Cosmochimica Acta*, **34**, 25–42.

Schwertmann, U. (1993) Relation between iron oxides, soil color, and soil formation. Pp. 51–69 in: *Soil Color* (J.M. Bigham and E.J. Ciolkosz, editors). Soil Science Society of America, Madison, Wisconsin, USA.

Şengör, A.M.C. and Yılmaz, Y. (1981) Tethyan evolution of Turkey: a plate tectonic approach. *Tectonophysics*, **75**, 181–241.

Seyitoğlu, G., Çemen, İ., and Tekeli, O. (2000) Extensional folding in the Alaşehir (Gediz) graben, western Turkey. *Journal of the Geological Society of London*, **157**, 1097–1100.

Sheppard, S.M.F., Nielsen, R.L., and Taylor, H.P. (1969) Oxygen and hydrogen isotope ratios of clay minerals from porphyry copper deposits. *Economic Geology*, **64**, 755–777.

Sheppard, S.M.F. and Gilg, H.A. (1996) Stable isotope geochemisty of clay minerals. *Clay Minerals*, **31**, 1–24.

Taylor, H.P. (1974) The application of oxygen and hydrogen isotope studies to problems of hydrothermal alteration and ore deposition. *Economic Geology*, **69**, 843–883.

Taylor, H.P. (1979) Oxygen and hydrogen relationships in hydrothermal mineral deposits. Pp. 236–277 in: *Geochemistry of Hydrothermal Ore Deposits* (H.L. Barnes, editor), 2nd edition. Wiley, New York.

Tauler, E., Proenza, J.A., Gal, S., Lewis, J.F., Labrador, M., Garcia-Romero, E., Suarez, M., Longo, F., and Bloise, G. (2009) Ni-sepiolite-falcondite in garnierite mineralization from the Falcondo Ni-laterite deposit, Dominican Republic. *Clay Minerals*, **44**, 435–454.

Thorne, R., Herrington, R., and Roberts, S. (2009) Composition and origin of the Çaldağ oxide nickel laterite, W. Turkey. *Mineralium Deposita*, **44**, 581–595.

Trescases, J.J. (1975) L'évolution géochimique supergène des roches ultrabasiques en zone tropicale. *ORSTOM Mémoires*, **78**, 259 pp.

Troly, G., Esterle, M., Pelletier, B., and Reibell, W. (1979) Nickel deposits in New Caledonia, some factors influencing their formation. Pp. 85–119 in: *International Laterite Symposium* (D.J.I. Evans, R.S. Shoemaker, and H. Veltman, editors). Society of Mining Engineers, New York.

Velbel, M.A. (2009) Dissolution of olivine during natural weathering. *Geochimica et Cosmochimica Acta*, **73**, 6098–6113.

Velbel, M.A. and Barker, W.W. (2008) Pyroxene weathering to smectite: conventional and cryo-field emission scanning electron microscopy, Koua Bocca ultramafic complex, Ivory Coast. *Clays and Clay Minerals*, **56**, 112–127.

Velbel, M.A., Donatelle, A.R., and Formolo, M.J. (2009) Reaction-product textures, volume relations, and implications for major-element mobility during natural weathering of hornblende, Tallulah Falls Formation, Georgia Blue Ridge, U.S.A. *American Journal of Science*, **309**, 661–688.

Venturelli, G., Gontini, S., Bonazzi, A., and Mangia, A. (1997) Weathering of ultramafic rocks and element mobility at Mt. Prinzera, Northern Apennines, Italy. *Mineralogical Magazine*, **61**, 765–778.

Wells, M.A., Ramanaidou, E.R., Verrall M., and Tessarolo, C. (2009) Mineralogy and chemistry of ''garnierites'' in the Goro lateritic nickel deposit, New Caledonia. *European Journal of Mineralogy*, **21**, 467–483.

Whitney, D.L. and Evans, B.W. (2010) Abbreviations for names of rock-forming minerals. *American Mineralogist*, **95**, 185–187.

Yıldız, M. and Bailey, E.H. (1978) *Mercury Deposits in Turkey*. United States Government Printing Office, Washington, D.C., 80 pp.

Yılmaz, Y., Genç, Ş.C., Gürer. F., Bozcu, M., Yılmaz, K., Karacık, Z., Altunkaynak, Ş, and Elmas, A. (2000) When did the western Anatolian grabens begin to develop? Pp. 353–384 in: *Tectonics and Magmatism in Turkey and the Surrounding Area* (E. Bozkurt, J.A. Winchester, and J.D.A Piper, editors). Special Publications **173**, Geological Society, London.

Yüksel, A.K. (2013) *Muratdağı Melanjı'nın Jeodinamik Özellikleri.* Balıkesir Üniversitesi, Fen Bilimleri Enstitüsü, Doktora Tezi (in Turkish, unpublished), 97 pp.

Zeissink, H.E. (1969) The mineralogy and geochemistry of a nickeliferous laterite profile (Greenvale, Queensland, Australia). *Mineralium Deposita*, **4**, 132–152.

(*Received 29 July 2014; revised 1 May 2015; Ms. 904; AE: M.A. Velbel*)